Seasonality fluctuations recorded in fossil bivalves during the early Pleistocene: implications for climate change

Gaia Crippa[1], L. Angiolini[1], C. Bottini[1], E. Erba[1], F. Felletti[1], C. Frigerio[1], J.A.I. Hennissen[2], M.J. Leng[3,4], M.R. Petrizzo[1], I. Raffi[5], G. Raineri[6] and M.H. Stephenson[2]

[1] *Università degli Studi di Milano, Dipartimento di Scienze della Terra 'A. Desio', via Mangiagalli 34, Milano, 20133, Italy. Corresponding author: gaia.crippa@unimi.it*

[2] *British Geological Survey, Keyworth, Nottingham, NG12 5GG, UK*

[3] *NERC Isotope Geosciences Facilities, British Geological Survey, Keyworth, Nottingham NG12 5GG, UK*

[4] *Centre for Environmental Geochemistry, School of Geography, University of Nottingham, Nottingham NG7 2RD, UK*

[5] *Università 'G. D'Annunzio', Dipartimento di Ingegneria e Geologia, via dei Vestini 31, Chieti Scalo, 66013, Italy*

[6] *Parco Regionale dello Stirone e del Piacenziano, Loc. Scipione Ponte 1, Salsomaggiore Terme, 43039, Italy*

Keywords: Sclerochemistry; stable isotope; Mediterranean Sea; fossil archive

ABSTRACT

Understanding the transformations of the climate system may help to predict and reduce the effects of global climate change. The geological record provides a unique archive that documents the long-term fluctuations of environmental variables, such as seasonal change. Here, we investigate how seasonal variation in seawater temperatures varied in the Mediterranean Sea during the early Pleistocene, approaching the Early-Middle Pleistocene Transition (EMPT) and the beginning of precession-driven Quaternary-style glacial-interglacial cycles. We performed whole-shell and sclerochemical stable isotope analyses ($\delta^{18}O$, $\delta^{13}C$) on bivalves, collected from

the lower Pleistocene Arda River marine succession (northern Italy), after checking shell preservation. Our results indicate that seawater temperature seasonality was the main variable of climate change in the Mediterranean area during the early Pleistocene, with the Northern Hemisphere Glaciation (NHG) exerting a control on the Mediterranean climate. We show that strong seasonality (14.4–16.0 °C range) and low winter paleotemperatures (0.8–1.6 °C) were likely the triggers leading to the establishment of widespread populations of so called “northern guests” (i.e., cold water taxa) in the Mediterranean Sea around 1.80 Ma. The shells postdating the arrival of the “northern guests” record a return to lower seasonal variations and higher seawater paleotemperatures, with seasonality increasing again approaching the EMPT; the latter, however, is not associated with a corresponding cooling of mean seawater paleotemperatures, showing that the observed seasonality variation represents a clear signal of progressive climate change in the Mediterranean Sea.

1. Introduction

In order to understand climate change and to predict and potentially reduce its impending effects, it is important to estimate the long-term natural variability of certain environmental variables (e.g., albedo, ice cover, ocean acidification, seawater temperature and seasonality) in the recent and distant past. The geological record provides a unique opportunity to document and scrutinize the effects of environmental variables on climate and ecosystem behaviors, including seasonal change.

Seasonality is a fundamental component of the climate system and has a strong influence on biotic distribution and evolution, in particular on human societies (Hansen et al., 2011). Hominid evolution was controlled by seasonality (Foley in Ulijaszek and Strickland, 1993). Resolving

seasonality during periods of climate change in the geological past has important implications for predicting and understanding the transformations which will affect human society in the future. Few studies have addressed the question of how seasonality varied during global climate change. During the Eocene–Oligocene greenhouse to icehouse transition, an increase in seasonality with constant mean paleotemperatures, was recorded by the isotope composition of fish otoliths (Ivany et al., 2000) and by spore and pollen assemblages (Eldrett et al., 2009). Denton et al. (2005) and Ferguson et al. (2011) showed that extreme seasonality occurred during the last glaciations and into the Holocene, respectively analyzing ice-core oxygen isotopes and limpet shells geochemistry. Recently, Hennissen et al. (2015), analyzed planktonic foraminifera paleotemperature records across the Neogene–Quaternary boundary (2.78–2.52 Ma) and observed an increase in seasonality with relatively stable summer paleotemperatures and with seasonality peaking during glacial intervals.

Here, we investigate how seasonality in Mediterranean seawater temperatures varied during the early Pleistocene (2.58–0.78 Ma; ICS, 2015), an interval characterized by climatic oscillations related to glacial/interglacial cycles. These climatic oscillations caused several cooling events, producing an increase in the ice cap thickness and significant sea level drops (e.g., Clark et al., 2006; Sosdian and Rosenthal, 2009; Elderfield et al., 2012). The beginning and end of this time interval coincide with two important climatic events: the intensification of the Northern Hemisphere Glaciation (NHG) ~2.6 Ma ago (Sosdian and Rosenthal, 2009) and the Early-Middle Pleistocene Transition (EMPT, 1.4–0.4 Ma; Head and Gibbard, 2015), which marks the onset of precession-driven Quaternary-style glacial-interglacial cycles (e.g., Clark et al., 2006; Ehlers and Gibbard, 2007; Sarnthein et al., 2009; Elderfield et al., 2012; Head and Gibbard, 2015).

The Mediterranean area was affected by early Pleistocene climatic changes both in marine and continental settings (e.g., Bertini, 2010; Fusco, 2010; Combourieu-Nebout et al., 2015). In the marine environment important biotic events are represented by the disappearance of warm water taxa and by the occurrence of “northern guests”, i.e. organisms such as the bivalve *Arctica islandica* and the foraminifera *Hyalinea balthica* and *Neogloboquadrina pachyderma* left-coiling, which lived and are living nowadays at higher northern latitudes and migrated into the Mediterranean Sea through the Strait of Gibraltar as a consequence of the cooling beginning in the Calabrian (Suess, 1883–1888; Raffi, 1986; Martínez-García et al., 2015). The first occurrence of “northern guests” in the Mediterranean Sea at ~1.806 Ma has an historical importance; it was used for the definition of the Pliocene–Pleistocene boundary (Aguirre and Pasini, 1985) at the former Global Stratotype Section and Point (GSSP) at Vrica (Calabria, Italy). The Pliocene–Pleistocene boundary has now been revised and lowered to 2.58 Ma at the base of the Gelasian Stage (e.g., Gibbard et al., 2010; ICS, 2015).

The Arda River marine succession, cropping out in northern Italy, continuously covers the early Pleistocene and is rich in macrofossils, representing an ideal setting to study how seawater temperature seasonality varied using the isotope composition of fossil bivalve shells. Bivalve shells are excellent archives of proxies which can be used to track past oceanic conditions (e.g., O'Neil et al., 1969; Schöne and Surge, 2012; Brocas et al., 2013) because they record the primary isotope composition of the seawater in which they lived with no vital effect (Hickson et al., 1999; Royer et al., 2013; Schöne, 2013). Also, they grow episodically rather than continuously and major growth lines or bands form due to seasonal perturbations, providing a tool to resolve annual variations (e.g., Ivany and Runnegar, 2010; Schöne and Surge, 2012).

To evaluate temperature seasonality in the Pleistocene Mediterranean we use a multidisciplinary approach based on sedimentology, isotope sclerochemistry ($\delta^{18}O_{sh}$, $\delta^{13}C_{sh}$) - "a sub-discipline of sclerochronology used to describe solely geochemical studies of the accretionary skeletal parts of fossil organisms" (Gröcke and Gillikin, 2008, p. 266) - and stable isotope composition of whole bivalve shells ($\delta^{18}O_{wh}$). This gives us the opportunity to analyze not only mean seawater paleotemperature/salinity changes, but also to explore how the seasonal seawater paleotemperature/salinity variations evolved through key intervals during the early Pleistocene.

2. Geological setting

The 237 m-thick Arda River marine succession belongs to the upper part of the Castell'Arquato Formation (Calabrese and Di Dio, 2009), which crops out in northern Italy along the Arda River at Castell'Arquato (Western Emilia) (Fig. 1). It comprises sandstones, siltstones and mudstones deposited in the Paleo-Adriatic in a tectonically active setting during phases of advance of fan deltas. It shows a general regressive trend punctuated by lower order transgressive and regressive cycles with shifts from infralittoral to shallow circalittoral environments, at water depths between 5 and 50 m. The base of the section is cut by a fault, causing the repetition of the first 37 m of the succession (base at 44°51'18.52''N; 9°52'26.7''E); the succession described here begins stratigraphically above the fault (Fig. 2E). The succession is bounded at the top by continental conglomerates that indicate a major sea level drop and the establishment of a continental environment with vertebrate faunas and freshwater mollusks, which is typical of Western Emilian Pliocene–Pleistocene successions (Cigala Fulgosi, 1976; Pelosio and Raffi, 1977; Ciangherotti et al., 1997).

The changes in both grain size and depositional environments have been taken as an indication of increased sedimentary input due to high uplift and erosion rates in the Apennines (Amorosi et al., 1996; Argnani et al., 2003), and indicate that the tectonic evolution between early and Middle Pleistocene of the northern Apennines was dominated by vertical motions (Argnani et al., 1997). Additional evidence in support of the increased Pleistocene uplift and erosion rates comes from estimates of sedimentation rates for the Po Plain basin infilling (Bartolini et al., 1996), which for the Middle Pleistocene are almost double the rates for the Pliocene (Argnani et al., 2003).

2.1. Age of the section: Calcareous nannofossil and foraminifera bio-chronostratigraphy

Based on original data on calcareous nannofossil and foraminifera biostratigraphy, here shown for the first time, the succession is assigned to the Calabrian Stage (early Pleistocene) ranging from ~1.8 to 1.2 Ma, as also supported by a previous study on the mollusk fauna (Crippa and Raineri, 2015).

2.1.1 Calcareous nannofossils

A total of 58 samples from the Arda section were analyzed for nannofossil biostratigraphy and abundance (Fig. 3; Table S1 in the Supplementary Material). The most important and common nannofossil taxa discussed in the paper are shown in Figure 4. Microscopic analyses were performed on smear slides under polarizing light, at 1250x magnification. Smear slides were prepared following the methodology described by Monechi and Thierstein (1985). For each sample, nannofossils were quantitatively characterized by counting at least 300 specimens. In addition, two random traverses were studied to detect rare and/or marker species. Specimen preservation is moderate to good throughout the entire studied interval (Table S1 in the Supplementary Material).

Calcareous nannofossil biozonations for the Cenozoic were developed by Martini (1971), Bukry (1973, 1975, 1978) and Okada and Bukry (1980), and were updated by Backman et al. (2012), who proposed the scheme used here. The identification of *Gephyrocapsa* specimens is based on the informal taxonomic concepts established by Raffi et al. (1993): "small" *Gephyrocapsa* refers to specimens <4 μm in size, "medium" *Gephyrocapsa* refers to specimens ≥4 μm, "large" *Gephyrocapsa* refers to specimens >5.5 μm.

The assemblages are characterized by the presence of small placoliths (e.g., reticulofenestrids and gephyrocapsids <4 μm in size), *Pseudoemiliania lacunosa*, *Calcidiscus macintyrei*, *Helicosphaera sellii* and, in some intervals, by *Gephyrocapsa* ≥4 μm, and/or *Gephyrocapsa* >5.5 μm. All these taxa are considered to be *in situ* (Fig. 3). In addition, reworked Cretaceous and Cenozoic species have been detected in relatively high abundance making up ca. 80% of the assemblage (Fig. 3). Specifically, the abundance of reworked Upper Cretaceous species is constant throughout the section (20%), while Lower Cretaceous species become more abundant (up to 5%) in the upper part of the section from 135 m. Reworked Cenozoic species are present throughout the section with an average of 24%. The presence of reworked species in the assemblages was likely supplied by the erosion of the Apennine chain to the Pleistocene Paleo-Adriatic basin.

The nannofossil events (First Occurrences - FOs, and Last Occurrences - LOs) recognized in the Arda section, allowed the identification of some of the biozones defined by Backman et al. (2012) and, consequently, the age determination of the studied part of the section (Figs. 2D, 3). Specifically, the following biozones were identified:

a) The interval from 37 to 111 m is assigned to Zone CNPL7 due to the presence of *Gephyrocapsa* <4 μm, and the absence of *Discoaster brouweri*. In this interval, the assemblage is also characterized by specimens of *H. sellii, C. macintyrei* and *P. lacunosa.*

b) The interval from 111 to 230 m is assigned to Zone CNPL8 (1.71–1.25 Ma) for the presence of *Gephyrocapsa* ≥4 μm at 111 m. At 180 m, the lowest occurrence of *Gephyrocapsa* >5.5 μm is recorded (dated 1.59 Ma). These "large" *Gephyrocapsa* specimens are found up to 230 m where their LO marks the top of Zone CNPL8.

c) The interval from 230 m to the top of the studied interval is assigned to the lower part of Zone CNPL9. In this interval specimens of *Gephyrocapsa* (<4 μm) occur concomitantly with relatively abundant *P. lacunosa* and few specimens of *H. sellii*. This suggests that the section extends into the lowermost part of Zone CNPL9 (below the LO of *H. sellii* and the FO of *Reticulofenestra asanoi*, dated at 1.14 Ma) and that the studied part of the Arda section is older than 1.14 Ma.

2.1.2 Foraminifera

Planktonic and benthic foraminifera were isolated from 48 samples which were soaked in tap water, washed under running water through >63 μm, >125 μm and >250 μm sieves and then dried. The washed residues contain varying amounts of quartz, mica, ostracods, mollusk and echinoid fragments, plant debris, iron oxides and aggregated grains. Foraminifera are common to abundant in all samples, with benthic forms generally occurring in greater abundance than planktonic forms. Residues were split into a fixed aliquot containing approximately 500–600 specimens; samples were scanned for the presence of biostratigraphic marker species when necessary.

Taxonomic concepts for species identification applied in this study follow Colalongo and Sartoni

(1977), AGIP (1982), Kennett and Srinivasan (1983), Iaccarino (1985), Iaccarino et al. (2007) and Holbourn et al. (2013). Selected species are illustrated in Figure 5. Foraminiferal biozonation follows Iaccarino et al. (2007) and Cita et al. (2012).

Benthic foraminifera are abundant and preservation is generally good. Samples include circalittoral assemblages with increased frequency of Buliminidae, Bolivinidae and Cassidulinidae, and infralittoral assemblages dominated by Rotalidae, Elphididae, Astigerinidae and Nonionidae with intercalated lagoon-brackish species (i.e., *Ammonia tepida*, *Elphidium granosum*). Generally, benthic foraminiferal assemblages reflect a wide variety of environments controlled by sea level oscillations that range from infralittoral to circalittoral, including infralittoral environments characterized by high nutrient input and freshwater influence. Further studies are in progress to provide a detailed paleoenvironmental interpretation based on variations in the foraminiferal assemblages.

Planktonic foraminifera are rare to frequent and usually small size. Preservation is generally good but becomes moderate to poor in the upper part of the section. The assemblages are generally composed of common *Globigerina bulloides*, *Globigerinoides elongatus*, *Globigerinoides obliquus*, *Globigerinoides ruber*, *Globigerina falconensis*, *Turborotalita quinqueloba* and *Orbulina universa*.

Common Paleogene and Pliocene planktonic foraminiferal taxa occur throughout the section, indicating a strong reworking from older stratigraphic levels. Reworked planktonic foraminiferal taxa include *Catapsydrax* spp., *Paragloborotalia* spp., *Globigerina venezuelana*, *Globorotaloides* spp., *Globorotalia crassaformis* gr. and *Globorotalia mediterranea*.

Nevertheless, we observe a reliable sequence of planktonic and benthic foraminiferal bioevents correlatable with the record of the Calabrian GSSP boundary stratotype of Vrica (see Cita et al.,

2012 and references herein) as described below in stratigraphic order.

The presence of rare specimens of *Globigerina cariacoensis* and of the benthic foraminifera *Uvigerina mediterranea* and *Uvigerina bradyana* at the base of the section (37.05 m), followed upward at 48 m by the lowest occurrence of the cold water adapted *Neogloboquadrina pachyderma* left-coiling, allows us to assign the Arda section to the Calabrian Stage (early Pleistocene) *Globigerina cariacoensis* Zone (Fig. 2D). Additional data are the highest occurrence of *Globigerinoides obliquus extremus* at 63 m, while the "northern guest" *Hyalinea balthica* is first recorded at 98.30 m. The presence of *Bulimina elegans marginata* and *Bulimina etnea* at 151 m further confirms an early Pleistocene age in agreement with data from previous studies in the Mediterranean area (e.g., Colalongo and Sartoni, 1979; Ragaini et al., 2006; Cosentino et al., 2009; Di Bella, 2010; Maiorano et al., 2010; Baldanza et al., 2011, among many others).

The age of the top of the section cannot be precisely constrained owing to the absence of marker bioevents (e.g., temporary disappearance of *N. pachyderma* left-coiling, lowest occurrence of *Truncorotalia truncatulinoides excelsa*). However, based on foraminiferal biostratigraphy and geochronology data from the Vrica section, the age of the studied stratigraphic interval is between 1.78 Ma at the base and about 1.1 Ma at the top (see Cita et al., 2012; Gradstein et al., 2012) (Fig. 2D).

3. Material: The bivalve fossil archive

The bivalves used in the present analyses belong to the species *Glycymeris glycymeris* (Linnaeus, 1758), *Glycymeris insubrica* (Brocchi, 1814), *Glycymeris inflata* (Brocchi, 1814), *Glycymeris* sp., *Aequipecten opercularis* (Linnaeus, 1758), *Aequipecten scabrella* (Lamarck, 1819) and

Arctica islandica (Linnaeus, 1767). These species have been shown to lack vital effects which make them suitable for stable isotope analyses and seasonal paleotemperature reconstructions (e.g., Hickson et al., 1999; Schöne et al., 2005; Brocas et al., 2013; Royer et al., 2013; Schöne, 2013; Bušelić et al., 2015). Shallow-water mollusks represent an accurate archive of paleoclimatic information, and have been successfully used for past climate reconstructions (e.g., Ivany et al. 2008; Huyghe et al., 2015), even if they can be influenced by salinity changes that affect $\delta^{18}O$ and thus the estimated paleotemperatures (Huyghe et al., 2015). To accurately interpret the data resulting from the isotope analyses it is thus important to take into account also the paleoecology of the studied species, focusing especially on those variables which can affect the isotope signals and their consequent interpretation, such as the living depth and the tolerance to salinity changes.

The species of *Glycymeris* identified in this study are known to be poor burrowers (Thomas, 1976), they are often found lying on the surface of the seabed or partially buried in sediments (Oliver and Holmes, 2006). *Glycymeris glycymeris* usually inhabits coarse sand and gravel substrates at depths of up to 100 m in water of normal marine salinity (Royer et al., 2013), whereas the extinct species *Glycymeris inflata* probably lived in gravel-sand deposits in water of normal marine salinity up to 70 m depth (Raineri, 2007). *Glycymeris insubrica* is the shallowest among the *Glycymeris* species occurring in the Arda succession, being abundant in medium-fine sand or mud deposits of the infralittoral zone (from 2.5 m to 40 m depth), but also in lagoonal settings (Malatesta, 1974; Lozano Francisco et al., 1993; Raineri, 2007; Crnčević et al., 2013); it is thus well adapted to tolerate salinity fluctuations.

The epifaunal species *A. opercularis* thrives in medium to fine grained sands, silts and shell gravels, at depth ranging from a few meters up to 180 m (Jimenez et al., 2009; Johnson et al.,

2009), tolerating only small salinity changes and constrained to a temperature range of about 5–24°C (Johnson et al., 2009). Less is known about the extinct taxon *A. scabrella*, but Jimenez et al. (2009) described it as a very generalist species.

In contrast with the above mentioned species, *A. islandica* is the only species living outside the Mediterranean Sea at the present. It thrives buried in muddy, sandy and gravelly sediments on continental shelves on both sides of the North Atlantic in Europe and North America (e.g., Witbaard, 1997), at water depth from 5 to more than 500 m (Schöne, 2013) with its short siphons just at the sediment-water interface (Lutz et al., 1981). In general it lives in water of normal marine salinity and has a temperature tolerance of 0–20°C (optimum temperature 6–16°C; Cargnelli et al., 1999). According to Raffi (1986) the ability of *A. islandica* to colonize widely is related more to the occurrence of low winter temperatures than to low summer ones.

4. Methods

4.1. Screening tests

The stable isotope composition of bivalve shell carbonate has been proven to be a very powerful tool for paleoclimatic and paleoenvironmental reconstructions (e.g., Schöne and Fiebig, 2009; Ivany and Runnegar, 2010; Royer et al., 2013; Beard et al., 2015). However, diagenetic processes may alter fossil bivalve shell isotope composition; for this reason it is important to check if the shell carbonate is pristine (i.e., unaltered from the time of growth). As shown by Brand et al. (2011) for other fossil archives, the best way of assessing the degree of alteration of an individual specimen is to apply as many screening tests as possible. We thus applied four different screening tests.

Scanning Electron Microscopy (SEM) (Fig. 6). We analyzed 245 fossil specimens with SEM. All the specimens were cut longitudinally along the axis of maximum growth (perpendicular to the growth lines). The obtained sections were then embedded in epoxy resin; every block was polished, ground-smooth and etched with 5% hydrochloric acid for 15–20 s in order to reveal the detail of the microstructure; finally, each block was gold-coated and studied with a Cambridge S-360 SEM with lanthanum hexaboride (LaB_6) cathodes at the University of Milan.

Cathodoluminescence (CL) (Fig. 7). To check if the shells are non-luminescent and thus adequately preserved (Barbin, 2000; England et al., 2006), bivalve shell sections were analyzed by CL at the University of Milan (Courtesy of F. Jadoul), using a Nuclide ELM2 cold cathode luminoscope operating at 10 kV and a beam current of 5–7 mA. Electron beam exposure (before taking the photo) was of the order of 15–30 s for all specimens to minimize damage to the micro-fabric. Photographic exposure time was set to 2 s for consistency using a Nikon Coolpix 4500 operating at 400 ISO.

X-Ray Powder Diffraction (XRD) (Fig. S1 in the Supplementary Material). A small amount of powder (~0.1 g) was collected from 65 bivalve shells, from species belonging to the genera *Glycymeris* and *Arctica*, using a microdrill (Dremel 3000) equipped with a 300-μm tungsten carbide drill bit. The powders were deposited on glass sample holders and fixed with acetone; finally, they were qualitatively analyzed with the X-ray powder diffractometer at the University of Milan (Courtesy of M. Dapiaggi) and the British Geological Survey (Keyworth, UK).

Feigl's solution (Feigl, 1937) (Fig. S2 in the Supplementary Material). Several aragonite and calcite bivalve shells were immersed in Feigl's solution for 30 minutes. At room

temperature, aragonite stains black if immersed in this solution for less than 30 minutes, whereas calcite remains unstained.

4.2. Isotope analyses

The oxygen isotope composition of shell carbonate (whole shell: $\delta^{18}O_{wh}$, sclerochemistry: $\delta^{18}O_{sh}$) was used to understand the evolution of temperature and water isotope composition (salinity and ice volume variations) through the succession (e.g., Epstein et al., 1953). The carbon isotope composition (sclerochemistry: $\delta^{13}C_{sh}$), although more complex to interpret, is thought to reflect paleosalinity and nutrient variations (Gillikin et al., 2006; McConnaughey and Gillikin, 2008).

For $\delta^{18}O_{wh}$, 249 fossil bivalve specimens belonging to species of *Glycymeris*, *Aequipecten* and *Arctica* (see section 3) from 141 stratigraphic intervals through the section were analyzed (Fig. 2C; Table S2 in the Supplementary Material); one valve of each specimen was brushed under deionized water, dried and cut longitudinally. One half was then crushed, using an agate pestle and mortar to a fine powder.

For $\delta^{18}O_{sh}$ and $\delta^{13}C_{sh}$, ten shells of *G. insubrica*, *G. inflata* and *A. islandica* were collected from six stratigraphic horizons and analyzed (Figs. 8, 9; Tables S3, S4 in the Supplementary Material). Valves were sliced along the axis of maximum growth, and 5 mm-thick sections were cut from each specimen and mounted on glass slides; they were smoothed with 400 and 1000 grit SiC powder, polished with 1 μm Al_2O_3 powder and cleaned with deionized water. The shells were then sampled at high resolution (spacing <1 mm) using a microdrill (Dremel 3000) equipped with a 300-μm tungsten carbide drill bit. Because growth rate decreases during the lifespan of bivalves (e.g., Goodwin et al., 2003), shells were sampled only in the first years of growth (AGI: number of annual growth increment sampled per shell, see Table 1) in order to sample the maximum growth rate interval and avoid mixing material from closely spaced annual bands. Up

to 12 samples were collected in each annual growth increment of the outer layer in the ontogenetically youngest portions of the shells (from 14 to 54 samples per shell).

For both whole shell and sclerochemical isotope analyses c. 50 micrograms of carbonate were dissolved in 100% phosphoric acid and the oxygen and carbon isotope ratios ($^{18}O/^{16}O$ and $^{13}C/^{12}C$) were measured using an Isoprime dual inlet mass spectrometer plus Multiprep device at the British Geological Survey, Keyworth (UK). Isotope values ($\delta^{18}O$, $\delta^{13}C$) are reported as per mil (‰) deviations of the isotope ratios ($^{18}O/^{16}O$ and $^{13}C/^{12}C$) calculated to the V-PDB scale using a within-run laboratory standard (KMC) calibrated against the international NBS standards (NBS18 and 19). Analytical reproducibility for these analyses was better than 0.1‰ for $\delta^{18}O$ and $\delta^{13}C$.

4.3 Stack correlation

The resulting Arda whole shell oxygen curve (Fig. 2C) was compared to the global benthic oxygen isotope stack of Lisiecki and Raymo (2005) (LR04; Fig. 2A) and to the planktonic Mediterranean stack (Lourens et al., 1996; Lourens, 2004; Wang et al., 2010; Fig. 2B). The graphic correlation of the Arda section with the LR04 and Mediterranean stacks was made using the lineage routine in Analyseries 2.0 (Paillard, 1996), constraining the interval from 1810 to 1220 ka, for a total duration of 590 ky over a depositional thickness of 200 m. Tie-points for the correlation were provided by nannoplankton biozonation (following Backman et al., 2012) and comparison to the LR04 benthic stack. Graphic correlation was attempted in areas where the sample density allowed the use of this technique, especially around 1600 ka.

The Arda whole shell oxygen curve is based on both aragonite and calcite shells, whereas the LR04 and Mediterranean stacks are based entirely on foraminiferal calcite. Oxygen isotope fractionation between aragonite-water and calcite-water is controversial: some authors (e.g.,

Tarutani et al., 1969; Böhm et al., 2000) observed that calcite is depleted in ^{18}O relative to aragonite, while others studies suggested the opposite (e.g., Epstein et al., 1953; Zhou and Zheng, 2003). In a recent paper, Lécuyer et al. (2012), analyzing mollusk species that secrete both aragonite and calcite layers in their shell, noted that biogenic aragonite is ^{18}O-enriched by 0.37‰ relative to coexisting biogenic calcite. However, this discrepancy was assigned to the difference in the acid fractionation factors between the two polymorphs digested at 90°C (Kim et al., 2007); therefore no oxygen fractionation is assumed between coexisting aragonite and calcite layers within the same mollusk shell.

4.4 Paleotemperature equation and estimate of seasonality

To calculate paleotemperatures from $\delta^{18}O_{sh}$, we used the modified equation of Grossman and Ku (1986), as reported in Schöne (2013), for species of *Arctica* and *Glycymeris*, which have an aragonite shell. A small modification of their equation was required because they report $\delta^{18}O_{sw}$ values in V-SMOW – 0.27% (see footnote 1 in Dettman et al., 1999):

$$T_{\delta^{18}O}\,(°C) = 20.60 - 4.34\,[\,\delta^{18}O_{aragonite} - (\delta^{18}O_{sw} - 0.27)\,]$$

where $\delta^{18}O_{aragonite}$ is measured relative to the Vienna PDB scale and $\delta^{18}O_{sw}$ is relative to the V-SMOW scale.

As there are no direct data for the $\delta^{18}O$ value of the seawater ($\delta^{18}O_{sw}$) in the early Pleistocene of the Mediterranean area, the value of $\delta^{18}O_{sw}$ has been assumed for each shell in each bed of the succession considering its position in the Arda oxygen curve compared to the LR04 and Mediterranean stacks (Fig. 2A–C; Table 1). For the shells from interglacials, a $\delta^{18}O_{sw}$ of 0.0‰ was assumed. This assumption is based on the fact that we cannot use the present (and thus interglacial) $\delta^{18}O_{sw}$ of the Mediterranean sea which is typically >+1.0‰ (Pierre, 1999), because evaporation rates today are higher than in the early Pleistocene, characterized by more humid

conditions (Fusco, 2007) and frequent fluvial runoff. For the shells from glacials, the value of $\delta^{18}O_{sw}$ has been assumed 0.8–1.0‰ higher than during an interglacial (following Schrag et al., 2002). When the shell was taken at the transition between two isotope stages, an intermediate value of 0.5‰ was used.

Seawater seasonality was estimated using two approaches (Table 1). First, we considered the larger amplitude cycle in $\delta^{18}O_{sh}$ ($\delta^{18}O_{sh\ max\text{-}excursion}$) which reflects the maximum seasonality recorded by each shell during the sampled interval; this was derived calculating the difference between the maximum ($\delta^{18}O_{sh\text{-}max}$) and minimum ($\delta^{18}O_{sh\text{-}min}$) oxygen isotope values of the larger amplitude cycle (Approach 1). Second, we averaged all defined maxima and minima from each annual increment in every shell (deriving values for $\delta^{18}O_{sh\ mean\text{-}max}$ and $\delta^{18}O_{sh\ mean\text{-}min}$), in order to obtain the mean $\delta^{18}O_{sh}$ variation ($\delta^{18}O_{sh\ mean\text{-}excursion}$) (Approach 2). For both approaches, we calculated the corresponding maximum (T_{max}, $T_{mean\text{-}max}$) and minimum (T_{min}, $T_{mean\text{-}min}$) paleotemperatures and temperature excursions ($T_{max\text{-}excursion}$, $T_{mean\text{-}excursion}$) using the modified equation of Grossman and Ku (1986). Both the approaches are likely to be conservative estimates as the full winter portion of the seasonal signal may not be represented (Beard et al., 2015). Although a potential error in absolute paleotemperature estimates based on assumed $\delta^{18}O_{sw}$ may exist, it is independent from annual paleotemperature ranges which are representative of seasonality.

5. Results

Four different screening tests were performed (SEM, CL, XRD and Feigl's solution). Overall the specimens used here are non-luminescent (pristine shells are usually non-luminescent, e.g., Popp et al., 1986; Grossman et al., 1993), their shell microstructure is exceptionally preserved

(showing no dissolution or recrystallization) and they comprise the original mineralogy. Rare specimens showed some alteration and were excluded from the analyses. We consider the bivalve shells analyzed to be pristine and suitable for isotope analyses (Figs. 6, 7; Figs. S1, S2 in the Supplementary Material).

5.1 Whole shell analysis

The whole shell oxygen isotope data ($\delta^{18}O_{wh}$) define a curve which shows $\delta^{18}O$ cyclical fluctuations through the Arda section (Fig. 2C; Table S2 in the Supplementary Material). The value of $\delta^{18}O_{wh}$ remains positive throughout the section (mean $\delta^{18}O_{wh}$ value: +1.7‰), except in its upper part, where it decreases to –1.6‰.

The bivalve record through the section is discontinuous, due to the nature of the macrofossil preservation; for this reason in some parts of the section we do not have enough data (as for example in the middle and upper part of the curve) to match the Arda whole shell oxygen isotope data to the marine stacks. However, there seems to be a better correlation with the LR04 stack rather than with the Mediterranean one, possibly because both the global and Arda curves are based on benthic organisms, while the Mediterranean stack is based on planktonic taxa (Fig. 2A–C).

5.2 Sclerochemical analysis

Isotope sclerochemical analyses reveal fluctuations of $\delta^{18}O_{sh}$ that closely match growth bands, with generally higher values recorded at the growth line (i.e., the junction between growth increments). Each shell contains 4–13 cycles, which reflect the seasonal change during the first years of bivalve growth.

The values of $\delta^{18}O_{sh}$ of *Arctica islandica* show a sinusoidal cyclicity, which is particularly pronounced in the bed of the first successfully established populations at 103.70 m (Bed 1 in Fig.

8; Table 1; Table S3 in the Supplementary Material). Here, the difference between the $\delta^{18}O_{sh\text{-}max}$ and $\delta^{18}O_{sh\text{-}min}$ values ($\delta^{18}O_{sh\ max\text{-}excursion}$) is 3.3–3.7‰, recording a strong seasonality ($T_{max\text{-}excursion}$) of about 14.4–16.0 °C and low minimum paleotemperatures (T_{min} 0.8–1.6 °C). The mean variation ($\delta^{18}O_{sh\ mean\text{-}excursion}$) recorded is 2.0–2.5‰, which corresponds to a mean paleotemperature seasonality ($T_{mean\text{-}excursion}$) of 8.7–10.9 °C. From 174 to 224.80 m (Beds 2–4 in Fig. 8), $\delta^{18}O_{sh\ max\text{-}excursion}$ first is lowered to 1.2‰, then increases to reach 2.7‰ and 1.6‰ in the upper beds ($T_{max\text{-}excursion}$ respectively of 5.2, 11.7 and 6.9 °C). The values of $\delta^{13}C_{sh}$ of *A. islandica* show less variation; peaks of $\delta^{13}C_{sh}$ occur in correspondence with peaks of $\delta^{18}O_{sh}$ (Fig. 8; Table S3 in the Supplementary Material). The mean oxygen values (MTS, obtained averaging the total isotope values in each shell) remain rather constant through the succession [2.9‰ and 2.5‰ (bed 1in Fig. 8), 3.0‰ (bed 2 in Fig. 8), 2.9‰ (bed 3 in Fig. 8)], except in bed at 224 m (Bed 4 in Fig. 8) where they are rather low (1.2‰) (Table 1).

At the base of the section, *G. inflata* shows low values of $\delta^{18}O_{sh\ max\text{-}excursion}$ (1.1‰) and $\delta^{18}O_{sh\ mean\text{-}excursion}$ (0.9‰), which correspond to low paleotemperature seasonality ($T_{max\text{-}excursion}$: 4.7 °C; $T_{mean\text{-}excursion}$: 3.9 °C) (Bed 1 in Fig. 9; Table 1; Table S4 in the Supplementary Material). From 174 m upwards specimens of *G. insubrica* show an increase in the cycle amplitudes, with $\delta^{18}O_{sh\ max\text{-}excursion}$ increasing from 1.6 to 4.4‰, corresponding to an increase in $T_{max\text{-}excursion}$ from 6.9 °C to 19.1 °C (Beds 2–4 in Fig. 9; Table 1; Table S4 in the Supplementary Material). Over the same interval, the values of $\delta^{18}O_{sh\ mean\text{-}excursion}$ show the same trend, increasing from 1.2 to 2.6‰ (corresponding increase in $T_{mean\text{-}excursion}$ from 5.2 to 11.2 °C). The overall decrease in $\delta^{18}O_{sh\text{-}min}$ (from +0.5 to –4‰) and in $\delta^{18}O_{sh\ mean\text{-}min}$ (from +0.6 to –3‰) of *Glycymeris* shells through the section is coupled with the lowering of mean oxygen data (MTS from +1.0 to –2.3‰), producing more negative $\delta^{18}O_{sh}$ values and thus higher paleotemperatures at the top (T_{max} up to 31.1 and

36.8 °C; $T_{mean\text{-}max}$ up to 30.3 and 32.4 °C) (Table 1). The variation of $\delta^{13}C_{sh}$ is more irregular and lower in amplitude than that of $\delta^{18}O_{sh}$; an upward decreasing trend is observed (mean $\delta^{13}C_{sh}$ from +2 to –0.1‰). Also, the highest peaks of $\delta^{13}C_{sh}$ slightly precede or are in correspondence with the highest peaks of $\delta^{18}O_{sh}$ (Fig. 9; Table S4 in the Supplementary Material).

When two specimens of *A. islandica* and *G. insubrica* were sampled from the same level [174 m (Bed 2 in Figs. 8, 9) and 224 m (Bed 4 in Fig. 8 and Bed 3 in Fig. 9) from the base of the section], the latter species shows higher amplitude oxygen cyclicity (Figs. 8, 9; Table 1). At 174 m (Bed 2 in Fig. 9) *G. insubrica* has $\delta^{18}O_{sh\ max\text{-}excursion}$ of 1.6‰ ($T_{max\text{-}excursion}$ of 6.9 °C) and $\delta^{18}O_{sh\ mean\text{-}excursion}$ of 1.2‰ ($T_{mean\text{-}excursion}$ of 5.2 °C), whereas *A. islandica* (bed 2 in Fig. 8) has $\delta^{18}O_{sh\ max\text{-}excursion}$ of 1.2‰ ($T_{max\text{-}excursion}$ of 5.2 °C) and $\delta^{18}O_{sh\ mean\text{-}excursion}$ of 1.0‰ ($T_{mean\text{-}excursion}$ of 4.3 °C). At 224 m *G. insubrica* (Bed 3 in Fig. 9) has $\delta^{18}O_{sh\ max\text{-}excursion}$ of 2.3‰ ($T_{max\text{-}excursion}$ of 10.0 °C) and $\delta^{18}O_{sh\ mean\text{-}excursion}$ of 1.3‰ ($T_{mean\text{-}excursion}$ of 5.7 °C), whereas *A. islandica* (Bed 4 in Fig. 8) has $\delta^{18}O_{sh\ max\text{-}excursion}$ of 1.6‰ ($T_{max\text{-}excursion}$ of 6.9 °C) and $\delta^{18}O_{sh\ mean\text{-}excursion}$ of 1.0‰ ($T_{mean\text{-}excursion}$ of 4.3 °C).

Finally, if we compare the values obtained averaging the total oxygen isotope values (MTS, Table 1) of the sclerochemical analysis in each shell with the corresponding whole shell datum used to build the oxygen curve, we observe a very small shift of nearly 0.5‰ between the two values; generally we found a higher value in the whole shell data, except for the specimens at the top of the section (AGC261-1, ACG261bis-1; Bed 4 in Fig. 9). This may be explained by the different sampling strategy used for sclerochemistry and whole shell. For whole shell analysis we averaged the data obtained from different taxa; furthermore we sampled the entire bivalve life span, where the pattern of growth may be influenced by the lower growth rates in the adulthood that biased the record of the warm season. Another explanation may be sought in the

incorporation of material from the inner shell layer - in the case of whole shell analysis -, which may not be in isotope equilibrium with the surrounding seawater, and thus, be responsible for this small difference between the two sets of data (Fig. 6 in Hickson et al., 1999). In any case, a shift of 0.5‰ between MTS and $\delta^{18}O_{wh}$ data should not be considered significant for our results.

6. Discussion

6.1. The record of *Arctica islandica*: seasonality changes

The $\delta^{18}O_{sh}$ of the first populations of the "northern guest" *A. islandica*, which were successfully established at 103.70 m (Bed 1 in Fig. 8), suggest that the Paleo-Adriatic was characterized by extreme seasonality ($T_{max\text{-}excursion}$: 14.4–16.0 °C; $T_{mean\text{-}excursion}$: 8.7–10.9 °C) and low winter paleotemperatures (T_{min}: 0.8–1.6 °C; $T_{mean\text{-}min}$: 4.2–6.8 °C) at this time. In fact, the observed pronounced $\delta^{18}O_{sh}$ oscillations cannot be ascribed to seasonal salinity variation, *A. islandica* being a stenohaline species. Instead, they reflect an intensification of seawater paleotemperature seasonality. Arda specimens of *Arctica islandica* were probably living below the thermocline (15–30 m in the northern Adriatic, Artegiani et al., 1997), where due to spring-summer water stratification, they were not affected by salinity changes.

Our measured values for both seasonal variation and winter paleotemperatures are not comparable with those of the present day shallow northern Adriatic Sea (seasonal variation at 20–25 m depth: 7 °C; minimum winter temperature: 9 °C; fig. 2 in Zavatarelli et al., 1998); in fact, the Arda shell seasonal variation is higher and winter paleotemperature lower than today for the specimens of *A. islandica* at 103.70 m where water depth was inferred to be 20–25 m. Therefore, the high seasonality recorded by the shells of *A. islandica* from this bed is mostly due to enhanced winter cooling, while summer temperatures remained relatively stable.

In the interval that postdates the arrival of "northern guests" (174–224 m, beds 2–4 in Fig. 8), *A. islandica* $\delta^{18}O_{sh}$ shows a slight increase in the amplitude of sinusoidal fluctuations, and thus in seasonality, toward the top of the section, with higher paleotemperatures and lower annual excursions (both $\delta^{18}O_{sh\ max\text{-}excursion}$ and $\delta^{18}O_{sh\ mean\text{-}excursion}$, see Table 1) than at 103.70 m. *Arctica islandica* records an increase of seawater paleotemperature seasonality, although with different intensity and pattern along the section. In particular, the establishment of "northern guests" at 103.70 m represents a turning point in the evolution of the region, a cold and high seasonality event which triggered the recruitment, reproduction and the successful establishment of "northern guests" in the Mediterranean Sea around 1.80 Ma. This is also supported by the presence of another "northern guest", the benthic foraminifera *Hyalinea balthica*, first occurring in the section at 98.30 m.

The arrival of the "northern guests" into the Mediterranean Sea (Kukla et al., 1979; Rio et al. in Van Couvering, 1997) is coeval with a pronounced drop in the abundance of the tropical planktonic foraminifera *Globigerinoides ruber* in the Mediterranean (Thunell et al., 1991), indicating seawater cooling at the beginning of the Calabrian. Winter paleotemperatures recorded by *A. islandica* shells are always lower if compared to present day winter temperatures in the northern shallow Adriatic (~8–9°C for the northern Adriatic at comparable living depth of the Arda specimens; see fig. 2 in Zavatarelli et al., 1998). However, the data from the Arda succession do not show a general seawater cooling trend through this time interval (1.8–1.2 Ma), but only an increase in seasonality. The MTS values of *A. islandica* (Table 1) remain rather constant through the succession, suggesting rather uniform mean seawater temperatures. The only exception to this pattern is given by the low value recorded by the stratigraphically highest specimen of *A. islandica* at 224 m (+1.2‰). However, the paleoecological and sedimentological

analyses of this bed indicate that this specimen of *A. islandica* was living at shallower depths and thus in warmer water than the specimens collected stratigraphically below. Therefore, *A. islandica* MTS values do not show any cooling in seawater paleotemperatures in the upper part of the succession, as might be expected approaching the EMPT and during the intensification of the NHG.

6.2. The record of the species of *Glycymeris*: temperature or salinity?

The shell of the stenohaline species *Glycymeris inflata*, collected below the bed of established populations of *A. islandica* (from the base of the section to 103.70 m), records a low seasonality ($T_{max\text{-}excursion}$: 4.7 °C, $T_{mean\text{-}excursion}$: 3.9 °C), which fits well with the present day seasonal temperature excursion in the shallow northern Adriatic Sea at 20 m water depth (plausible living depth below the thermocline of the specimen of *G. inflata* in the Arda section); this shell records the background paleoclimatic conditions before the successful establishment of the "northern guests" and the Apennine uplift, confirming the distinctiveness of the cold and high seasonality event at 103.70 m described above.

The shells belonging to the other species of *Glycymeris* (103.70 m – top of the section), the euryhaline *G. insubrica*, document an increase in the amplitude of the sinusoidal fluctuations of $\delta^{18}O_{sh}$ and thus an increase in seasonality from 174 m (Bed 2 in Fig. 9) toward the top of the section with $T_{max\text{-}excursion}$ increasing from 6.9 to 19.1 °C, and $T_{mean\text{-}excursion}$ from 5.2 to 11.2 °C. This increase in $\delta^{18}O_{sh\ max\text{-}excursion}$ (and also of $\delta^{18}O_{sh\ mean\text{-}excursion}$) of *G. insubrica* shells parallels at shallower water depths (5–10 m, above the thermocline) the one recorded at greater water depth by *A. islandica*, although with a higher excursion. The different living paleodepths between *G. insubrica* and *A. islandica* account for the higher $\delta^{18}O_{sh}$ amplitude cyclicity recorded

by *G. insubrica* when the two shells occur together in the same level (174 m and 224 m). In fact, taphonomic data suggest that *G. insubrica* was probably transported from nearby shallower settings to deeper environments, where *A. islandica* was thriving. Because it originated from shallower water settings, it records a higher seasonal variation. The high seasonal variation identified, enhanced by supposedly high summer paleotemperatures (at the top of the section: T_{max} up to 36.8 °C and $T_{mean\text{-}max}$ up to 32.4 °C), may reflect the interplay of temperature and salinity in shaping the $\delta^{18}O_{sh}$ signals of *G. insubrica* shells, a species which tolerates well salinity changes (e.g., Malatesta, 1974; Lozano Francisco et al., 1993; Raineri, 2007; Crnčević et al., 2013). Our calculated paleotemperatures are higher than the present day maximum summer temperatures in the shallow northern Adriatic Sea (23–24 °C at 5 m water depth, fig. 2 in Zavatarelli et al., 1998; depth comparable with the living depth of specimens of *G. insubrica* in the upper part of the section, from 230.80 m), suggesting that the $\delta^{18}O_{sh}$ record of *G. insubrica* was not only controlled by temperature.

We note a progressive decrease in $\delta^{18}O_{sh\text{-}min}$ (from +0.5 to –4.0‰) and $\delta^{18}O_{sh\ mean\text{-}min}$ (from +0.6 to –3.0‰) values toward the upper part of the section, indicating that a paleosalinity drop may have played a role, producing more negative $\delta^{18}O_{sh}$ in *G. insubrica* shells and apparently higher paleotemperatures, especially at the top of the section. From 230.80 m upward the occurrence of *G. insubrica*, together with only a few species tolerant of salinity variations (Crippa and Raineri, 2015), indicates that the uppermost shallow water paleocommunities may have been more prone to riverine influx and, by living at shallower water depth record higher seasonal variations.

The change in salinity was mainly due to an increase in riverine freshwater influx during the warmer seasons. Today, salinity decrease in the Adriatic surface waters due to riverine influx is more pronounced in spring and summer (Zavatarelli et al., 1998). Low $\delta^{13}C_{sh}$ corresponds to low

$\delta^{18}O_{sh}$, supporting riverine input in spring–summer, causing in turn the development of phytoplankton blooms in autumn–winter (Zavatarelli et al., 1998). These blooms extract more ^{12}C from seawater (leaving it enriched in ^{13}C) and may explain why $\delta^{13}C_{sh}$ peaks slightly precede (*Glycymeris* shells), or are in correspondence with (*Glycymeris* and *Arctica* shells), $\delta^{18}O_{sh}$ peaks. A salinity change of 2 psu corresponds to a shift of ~1‰ in $\delta^{18}O_{sw}$ (Rohling and Bigg, 1998), which is equivalent to nearly 4–5°C in the temperatures calculated from the shell oxygen isotope composition. Today, relative salinity fluctuations in the northern Adriatic are up to 4 psu in the top 10 m of the water column (Zavatarelli et al., 1998), thus their effect on $\delta^{18}O_{sw}$ would lead to calculated paleotemperatures up to 8–10 °C higher than the effective ones, especially during the warm season. Seasonal $\delta^{18}O_{sw}$ fluctuations (mostly caused by salinity) would have amplified the cyclicity of $\delta^{18}O_{sh}$. However, even with the impact of salinity change taken into consideration, an increasing trend in temperature seasonality is recorded also by the species of *Glycymeris*, corresponding to that recorded by *A. islandica* in deeper normal salinity water.

Therefore, the evidence suggests that the *G. inflata* record is controlled mainly by paleotemperature seasonality, as it lived in deeper water of normal salinity. The record of *G. insubrica* is partially controlled by paleotemperature, but also by paleosalinity which drops due to increased input of fresh water during the warmer months, especially from 230.80 m upward. However, the exact degree to which ^{18}O-depleted freshwater runoff is enhancing calculated summer paleotemperatures and seasonal variation is currently not possible to constrain.

In terms of MTS values, those of the shells of *Glycymeris* species record a trend toward lower values at the top of the succession (from +1.0 to –2.3‰), which may suggest warming (Table 1). However, we interpret this warming to be only apparent, and probably caused by the shallowing upward trend of the sedimentary succession, coupled with a major contribution of freshwater

input (causing salinity reduction) at the top of the succession; freshwater input lowers the MTS values recorded by the euryhaline *G. insubrica* specimens. This seems to be the most important controlling factor from 230.80 m to the top of the succession, as testified by several lines of evidence, in particular the increase of hyperpycnal deposits, created when a river in flood directly discharges a sustained and relatively more dense turbulent mixture of fresh water and sediments into a receiving standing body of water (Bates, 1953). The increase in terrigenous input caused by fluvial floods is related to an increase in the Apennine uplift and erosion (Bartolini et al., 1996). Increased freshwater input is also indicated by the presence of abundant brackish-water benthic foraminifera at the top of the succession and by the occurrence in the upper part of the section (from 230.80 m to the top) of only *Glycymeris insubrica*, a species which tolerates salinity variations (e.g., Malatesta, 1974; Lozano Francisco et al., 1993; Raineri, 2007; Crnčević et al., 2013). Finally, further evidence is given by a decrease in the mean $\delta^{13}C_{sh}$ recorded by *Glycymeris* shells (from +2 to –0.1‰) from the base to the top of the section; as fresh water is generally depleted in ^{13}C (due to the input of ^{12}C derived from the decomposition of terrestrial plants) a drop in salinity will cause a decrease in $\delta^{13}C$. All these findings explain the MTS trend toward lower values observed from 230.80 m to the top of the succession by *G. insubrica* shells, which is not caused by warming, but by salinity reduction. Nevertheless, the most evident outcome is that, aside from the upper part of the section, mean paleotemperatures through the section do not record any cooling approaching the EMPT.

6.3 Can paleoceanography offer an explanation for the observed paleobiogeographic pattern and seasonality change?

Herbert et al. (2015), using the alkenone unsaturation methodology, observed a pronounced cooling at 2.09–2.05 Ma in the Mediterranean Sea, followed by an abrupt onset of multiple cold episodes starting from ~1.84 Ma. During the Pliocene–Pleistocene, cold currents from the North Atlantic entered the Mediterranean Sea with annual-interannual frequency (e.g., Cacho et al., 2000; Becker et al., 2006), causing a gradual seawater cooling. The abrupt change observed around 2.00–1.80 Ma in the Mediterranean may suggest that a cooling threshold was reached and crossed, acting as a trigger factor for the arrival of the "northern guests". In particular, cold current inflows may have increased around 1.80 Ma when the sub-Arctic region underwent a substantial cooling and sea-ice expansion (Martínez-Garcia et al., 2010), which led to the formation and advection of cold waters flowing from the Northern Hemisphere seas further south to the North Atlantic and Mediterranean Sea (Sosdian and Rosenthal, 2009). This sub-Arctic ice expansion is indirectly linked to the NHG dynamics, which at this time exerted a control on seawater temperatures and had a far-field record in the Mediterranean. This is supported by previous studies, that showed that the NHG affected both continental and marine environments in the Mediterranean region (e.g., Becker et al., 2005, 2006; Herbert et al., 2015), thus producing strong feedbacks also outside the glaciated regions.

Moreover, considering that the northern Adriatic Sea is today a site of dense and deep water formation (Cacho et al., 2000), cold currents from the North Atlantic and cold air incursions linked to the NHG could have enhanced the process. Because dense, cold and more saline water formation occurred during winter months, we hypothesize that the high seasonality recorded in the shells of *A. islandica* at 103.70 m (Bed 1 in Fig. 8) is mostly due to stable summer paleotemperatures but enhanced winter cooling, which triggered the recruitment and the

successful establishment of “northern guests” populations (e.g., *Arctica islandica* and *Hyalinea balthica*) in the Mediterranean Sea around 1.80 Ma.

This was followed by a return to a lower seasonal variation and then by an intensification of seawater paleotemperature seasonality that culminates in the uppermost marine sediments at the top of the section, just below the transition to the continental deposits, with no record of a concomitant cooling in the mean seawater paleotemperatures. Rapid uplift of the Apennine chain after 1.80 Ma (e.g., Amorosi et al., 1996; Bartolini et al., 1996; Argnani et al., 1997, 2003; Dominici, 2001), may have acted as a shield for cold continental air masses coming from the Northern Hemisphere and entering the Mediterranean from the north and the west, producing a strong orographic influence on the local climate. From about 110 m upward the Arda section records an increase in terrigenous input and in nannofossil total abundance and composition, which may be indicative of ongoing tectonic activity (Figs. 2, 3; Table S1 in the Supplementary Material). Specifically, we observe that reworked Lower Cretaceous species show an increase in mean abundance at 135 m, likely deriving from the erosion of older sediments uplifted with the Apennine chain (Fig. 3; Table S1 in the Supplementary Material). Cold marine currents continued to flow into the Mediterranean Sea from the North Atlantic and dense and cold water kept on forming in the Adriatic Sea; however, the tectonic activity has to some degree obscured the impact of the climatic variations (reduction in mean paleotemperatures) linked to the NHG, especially by blocking those cold air incursions which are topographically channeled into the northwestern Mediterranean (Kuhlemann et al., 2008). Even though the Apennine uplift may have obscured the cooling caused by the NHG, the signal of progressive climate change is still present in bivalve shells in the form of increased seasonality.

7. Conclusion: is seasonality a good predictor for climate change?

The Arda River marine succession is Calabrian (early Pleistocene) in age, based on calcareous nannofossil and foraminifera biostratigraphy, which allow to identify respectively three nannofossil (CNPL7, CNPL8 and CNPL9) and one foraminiferal (*Globigerina cariacoensis*) biozones.

The main outcome of the isotope analyses performed on lower Pleistocene Arda bivalves is that seawater paleotemperature seasonality was the main variable involved in the climate change in the Mediterranean area during the early Pleistocene. In fact, the establishment of widespread populations of the "northern guest" *A. islandica* in the Mediterranean Sea around 1.80 Ma was triggered by extreme seawater temperature seasonality and low winter paleotemperatures, representing a turning point in the evolution of the region with the NHG dynamics exerting a strong influence at this time. After a return to lower seasonal variations and higher seawater paleotemperatures, similar to the background conditions recorded by *G. inflata* at the base of the section, seasonality increased again approaching the EMPT and the beginning of precession-driven Quaternary-style glacial-interglacial cycles in the Northern Hemisphere. This second increase in seasonality - recorded both by *A. islandica* and *G. insubrica* - was, however, not associated with a corresponding cooling of the mean seawater paleotemperatures. The Apennine uplift may have locally mitigated the influence of NHG on the Mediterranean climate, in particular on mean seawater paleotemperatures. All these data, however, indicate that the variation in seasonality represents a clear signal of progressive climate change in the Mediterranean Sea. In fact, an intensification of seasonality with constant mean paleotemperatures is seen also in other time intervals (e.g., Ivany et al., 2000; Eldrett et al., 2009), promoting seasonality as an important variable during climate change.

In addition, it has been noted that an increase in seasonality is often associated with cold, rather than with warm climate conditions, as observed also in other time intervals from the Cretaceous to the Holocene (e.g., Ivany et al., 2000; Pross and Klotz, 2002; Steuber et al., 2005; Ferguson et al., 2011; Hennissen et al., 2015); in particular a large seasonal variability is needed for the existence and maintenance of polar ice sheets (Steuber et al., 2005). Our observed increasing seasonality may have prepared the ground for the onset and establishment of eccentricity-controlled waxing and waning of the Middle and Upper Pleistocene continental glaciations. Overall, this study highlights the importance of resolving long-term seasonality changes, using fossil carbonate shells as paleoclimatic archives during different intervals of climate change in the recent and distant past in order to understand and predict long run transformations of the climate system.

ACKNOWLEDGMENTS

We would like to thank C. Malinverno and G. Pezzi for technical assistance and sample preparation. MRP wishes to thank S. Iaccarino, E. Turco (University of Parma) and M. Kucera (University of Bremen) for valuable information on Mediterranean foraminifera. We warmly thank A.L.A. Johnson and W. Brocas for their critical reading and their useful comments, which improved the manuscript. Two anonymous reviewers are also thanked for their comments and suggestions. The research was supported by 2011 Italian Ministry PRIN Project to E. Erba and funding from the British Geological Survey.

REFERENCES CITED

Agip S.p.A., 1982, Foraminiferi Padani (Terziario e Quaternario): Atlante iconografico e distribuzione stratigrafica. Seconda edizione. Milano.

Aguirre, E. and Pasini, G., 1985, The Pliocene–Pleistocene boundary: Episodes, v. 8, p. 116–120.

Amorosi, A., Farina, M., Severi, P., Preti, D., Caporale, L. and Di Dio, G., 1996, Genetically related alluvial deposits across active fault zones: an example of alluvial fan-terrace correlation from the upper Quaternary of the Southern Po Basin Italy: Sedimentary Geology, v. 102, p. 275–295.

Argnani, A., Bernini, M., Di Dio, G.M., Papani, G. and Rogledi, S., 1997, Stratigraphic record of crustal-scale tectonics in the Quaternary of the Northern Apennines (Italy): Il Quaternario, v. 10, p. 595–602.

Argnani, A., Barbacini, G., Bernini, M., Camurri, F., Ghielmi, M., Papani, G., Rizzini F., Rogledi, S. and Torelli L., 2003, Gravity tectonics driven by Quaternary uplift in the Northern Apennines: insights from the La Spezia-Reggio Emilia geo-transect: Quaternary International, v. 101–102, p.13–26.

Artegiani, A., Bregant, D., Paschini, E., Pinardi, N., Raicich, F. and Russo, A., 1997, The Adriatic Sea General Circulation. Part I: Air–Sea Interactions and Water Mass Structure: Journal of physical oceanography, v. 27, p. 1492–1514.

Backman, J., Raffi, I., Rio, D., Fornaciari, E. and Pälike, H., 2012, Biozonation and biochronology of Miocene through Pleistocene calcareous nannofossils from low and middle latitudes: Newsletters on Stratigraphy, v. 45, no. 3, p. 221–244.

Baldanza, A., Bizzarri, R. and Hepach, H., 2011, New biostratigraphic data from the Early Pleistocene tyrrhenian palaeocoast (western Umbria, central Italy): Geologia Croatica, v. 64, no. 2, p. 133–142.

Bartolini, C., Caputo, R. and Pieri, M., 1996, Pliocene-Quaternary sedimentation in the Northern Apennine Foredeep and related denudation: Geological Magazine, v. 133, p. 255–273.

Barbin, V., 2000, Cathodoluminescence of carbonate shells: biochemical vs. diagenetic process, In: Pagel, M., Barbin, V., Blanc, P, and Ohnenstetter, D. (eds) Cathodoluminescence in geosciences, Springer-Verlag, Berlin, p. 303–329.

Bates, C., 1953, Rational theory of delta formation: AAPG Bulletin, v. 37, p. 2119–2162.

Beard, J.A., Ivany, L.C., and Runnegar, B., 2015, Gradients in seasonality and seawater oxygen isotopic composition along the early Permian Gondwanan coast, SE Australia: Earth and Planetary Science Letters, v. 425, p. 219–231.

Becker, J., Hilgen, F.J., Lourens, L.J., Reichart, G.-J., van der Laan, E., and Kouwenhofen, T.J., 2005, Late Pliocene climate variability on Milankovitch to millennial time scales: A high-resolution study of MIS100 from the Mediterranean: Palaeogeography Palaeoclimatology Palaeoecology, v. 228, p. 338–360.

Becker, J., Lourens, L.J., and Raymo, M.E., 2006, High-frequency climate linkages between the North Atlantic and the Mediterranean during marine oxygen isotope stage 100 (MIS100): Paleoceanography, v. 21, PA3002, doi:10.1029/2005PA001168.

Bertini, A., 2010, Pliocene to Pleistocene palynoflora and vegetation in Italy: state of the art: Quaternary International, v. 225 (1), p. 5–24.

Böhm, F., Joachimski, M.M., Dullo, W.C., Eisenhauer, A., Lehnert, H., Reitner, J., and Worheide, G., 2000, Oxygen isotope fractionation in marine aragonite of coralline sponges: Geochimica et Cosmochimica Acta, v. 64, p. 1695–1703.

Brand, U., Logan, A., Bitner, M.A., Griesshaber, E., Azmy, K., and Buhl, D., 2011, What is the ideal proxy of Palaeozoic seawater chemistry?: Memoirs of the Association of Australasian Palaeontologists, v. 41, p. 9–24.

Brocas, W.M., Reynolds, D.J., Butler, P.G., Richardson, C.A., Scourse, J.D., Ridgway, I.D., and Ramsay, K., 2013, The dog cockle, *Glycymeris glycymeris* (L.), a new annually-resolved sclerochronological archive for the Irish Sea: Palaeogeography, Palaeoclimatology, Palaeoecology, v. 373, p. 133–140.

Brocchi, G.B., 1814, Conchiologia fossile subappennina. 2 vol. of 712 pp. Stamperia Reale, Milano.

Bukry, D., 1973, Low Latitude Coccolith Biostratigraphic Zonation, in Edgar, N.T., Saunders, J.B., et al., (eds.), Initial Reports DSDP 15: Washington, U.S. Government Printing Office, v. 15, p. 685–703.

Bukry, D., 1975, Coccolith and silicoflagellate stratigraphy, northwestern Pacific Ocean, Deep Sea Drilling Project Leg 32, in Larson, R.L., Moberly, R., et al., (eds.), Initial Reports DSDP 32: Washington, U.S. Government Printing Office, p. 677–701.

Bukry, D., 1978, Biostratigraphy of Cenozoic marine sediments by calcareous nannofossils: Micropaleontology, v. 24, p. 44–60.

Bušelić, I., Peharda, M., Reynolds, D.J., Butler, P.G., González, A.R., Ezgeta-Balić, D., Vilibić, I., Grbec, B., Hollyman, P., and Richardson, C.A., 2015, *Glycymeris bimaculata* (Poli, 1795) - A

new sclerochronological archive for the Mediterranean?: Journal of Sea Research, v. 95, p. 139–148.

Cacho, I., Grimalt, J.O., Sierro, F.J., Shackleton, N., and Canals, M., 2000, Evidence for enhanced Mediterranean thermohaline circulation during rapid climatic coolings: Earth and Planetary Science Letters, v. 183, p. 417– 429.

Calabrese, L., and Di Dio, G., 2009, Note Illustrative della Carta Geologica d'Italia alla scala 1: 50.000, foglio 180 “Salsomaggiore Terme”: Servizio Geologico d'Italia-Regione Emilia Romagna, Roma.

Cargnelli, L.M., Griesbach, S.J., Packer, D.B., and Weissberger, E., 1999, Ocean quahog, *Arctica islandica*, life history and habitat characteristics: NOAA Technical Memorandum NMFS-NE-148. p. 1–12.

Ciangherotti, A.D., Crispino, P., and Esu, D., 1997, Paleoecology of the non-marine molluscs of the Pleistocene Stirone River sequence (Emilia, Northern Italy): Bollettino della Società Paleontologica Italiana, v. 36, p. 303–310.

Cigala Fulgosi, F., 1976, *Dicerorhinus hemitoechus* (Falconer) del post-Villafranchiano fluvio lacustre del T. Stirone (Salsomaggiore, Parma): Bollettino della Società Paleontologica Italiana, v. 15 (1), p. 59–72.

Cita, M.B., Gibbard, P.L., Head, M.J., and the ICS subcommission on Quaternary Stratigraphy, 2012, Formal ratification of the GSSP for the base of the Calabrian Stage (second stage of the Pleistocene Series, Quaternary System): Episodes, v. 35, no. 3, p. 388–397.

Clark, P.U., Archer, D., Pollard, D., Blum, J.D., Rial, J.A., Brovkin, V., Mix, A.C., Pisias, N.G., and Roy, M., 2006, The middle Pleistocene transition: characteristics, mechanisms, and

implications for long-term changes in atmospheric pCO_2: Quaternary Science Reviews, v. 25, p. 3150–3184.

Colalongo, M.L., and Sartoni, S., 1977, *Globigerina calabra* nuova specie presso il limite Plio-Pleistocene della sezione della Vrica (Calabria): Giornale di Geologia, v. 42, p. 205–220.

Colalongo, M.L., and Sartoni, E., 1979, Schema biostratigrafico per il Pliocene ed il Pleistocene in Italia: Contributi Preliminari alla Carta Neotettonica d'Italia, v. 251, p. 645–654.

Combourieu-Nebout, N., Bertini, A., Russo-Ermolli, E., Peyron, O., Klotz, S., Montade, V., Fauquette, S., Allen, J., Fusco, F., Goring, S., Huntley, B., Joannin, S., Lebreton, V., Magri, D., Martinetto, E., Orain, R., and Sadori, L., 2015, Climate changes in the central Mediterranean and Italian vegetation dynamics since the Pliocene: Review of Palaeobotany and Palynology, v. 218, p. 127–147.

Cosentino, D., Cipollari, P., Di Bella, L., Esposito, A., Faranda, C., Giordano, G., Gliozzi, E., Mattei, M., and Mazzini, I., 2009, Tectonics, sea-level changes and paleoenvironments in the early Pleistocene of Rome (Italy): Quaternary Research, v. 72, p. 143–155.

Crippa, G., 2013, The shell ultrastructure of the genus *Glycymeris* Da Costa, 1778: a comparison between fossil and recent specimens: Rivista Italiana di Paleontologia e Stratigrafia, v. 119(3), p. 387–399.

Crippa, G., and Raineri, G., 2015, The genera *Glycymeris, Aequipecten* and *Arctica*, and associated mollusk fauna of the Lower Pleistocene Arda River section (Northern Italy): Rivista Italiana di Paleontologia e Stratigrafia, v. 121, no. 1, p. 61–101.

Crnčević, M., Balić, D.E., and Pećarević, M., 2013, Reproductive cycle of *Glycymeris nummaria* (Linnaeus, 1758) (Mollusca: Bivalvia) from Mali Ston Bay, Adriatic Sea, Croatia: Scientia marina, v. 77 (2), p. 293–300.

Denton, G.H., Alley, R.B., Comer, G.C., and Broecker, W.S., 2005, The role of seasonality in abrupt climate change: Quaternary Science Reviews, v. 24, no. 10–11, p. 1159–1182.

Dettman, D.L., Reische, A.K., and Lohmann, K.C., 1999, Controls on the stable isotope composition of seasonal growth bands in aragonitic fresh-water bivalves (Unionidae): Geochimica et Cosmochimica Acta, v. 63, p. 1049–1057.

Di Bella, L., 2010, Plio-Pleistocene foraminiferal assemblages of the Monte Mario site (Rome, Italy): Bollettino della Società Paleontologica Italiana, v. 49, p. 145–161.

Dominici, S., 2001, Taphonomy and paleoecology of shallow marine macrofossil assemblages in a collisional setting (late Pliocene–early Pleistocene, western Emilia, Italy): PALAIOS, v. 16, p. 336–353.

Ehlers, J., and Gibbard, P.L., 2007, The extent and chronology of Cenozoic global glaciation: Quaternary International, v. 164, p. 6–20.

Elderfield, H., Ferretti, P., Greaves, M., Crowhurst, S., McCave, I.N., Hodell, D., and Piotrowski, A.M., 2012, Evolution of ocean temperature and ice volume through the Mid-Pleistocene climate transition: Science, v. 337 (6095), p. 704–709.

Eldrett, J.S., Greenwood, D.R., Harding, I.C., and Huber, M., 2009, Increased seasonality through the Eocene to Oligocene transition in northern high latitudes: Nature, v. 459, p. 969–973.

England, J., Cusack, M., Paterson, N.W., Edwards, P., Lee, M.R., and Martin, R., 2006, Hyperspectral cathodoluminescence imaging of modern and fossil carbonate shells: Journal of Geophysical Research, v. 111, G03001, doi:10.1029/2005JG000144.

Epstein, S., Buchsbaum, R., Lowenstam, H.A., and Urey, H.C., 1953, Revised carbonate – water isotopic temperature scale: Bulletin of the Geological Society of America, v. 64, p. 1315–1326.

Feigl, F., 1937, Qualitative analysis by spot tests, Nordemann Publishing Company, New York, 400 pp.

Ferguson, J.E., Henderson, G.M., Fa, D.A., Finlayson, J.C., and Charnley, N.R., 2011, Increased seasonality in the Western Mediterranean during the last glacial from limpet shell geochemistry: Earth and Planetary Science Letters, v. 308, no. 3-4, p. 325–333.

Fusco, F., 2007, Vegetation response to early Pleistocene climatic cycles in the Lamone valley (Northern Apennines, Italy): Review of Palaeobotany and Palynology, v. 145 (1), p. 1–23.

Fusco, F., 2010, *Picea* + *Tsuga* pollen record as a mirror of oxygen isotope signal? An insight into the Italian long pollen series from Pliocene to Early Pleistocene: Quaternary International, v. 225 (1), p. 58–74.

Gibbard, P.L., Head, M.J., and Walker, M.J., 2010, Formal ratification of the Quaternary System/Period and the Pleistocene Series/Epoch with a base at 2.58 Ma: Journal of Quaternary Science, v. 25, p. 96–102.

Gillikin, D.P., Lorrain, A., Bouillon, S., Willenz, P., and Dehairs, F., 2006, Stable carbon isotope composition of *Mytilus edulis* shells: Relation to metabolism, salinity, $\delta^{13}C_{DIC}$, and phytoplankton: Journal of Organic Geochemistry, v. 37, p. 1371–1382.

Goodwin, D., Schöne, B., and Dettman, D., 2003, Resolution and fidelity of oxygen isotopes as paleotemperature proxies in bivalve mollusc shells: models and observations: Palaios, v. 18, p. 110–125.

Gradstein, F.M., Ogg, J.G., Schmitz, M.D., and Ogg, G.M., 2012, The geologic time scale 2012: Oxford, UK, Elsevier, 1144 p.

Gröcke, D.R., and Gillikin, D.P., 2008, Advances in mollusc sclerochronology and sclerochemistry: tools for understanding climate and environment: Geo-Marine Letters, v. 28 (5-6), p. 265–268.

Grossman, E.L., and Ku, T.L., 1986, Oxygen and carbon isotope fractionation in biogenic aragonite - temperature effects: Chemical Geology, v. 59, p. 59–74.

Grossman, E.L., Mii, H.S., and Yancey, T.E., 1993, Stable isotopes in Late Pennsylvanian brachiopods from the United States : implications for Carboniferous paleoceanography: Geological Society of America, Bulletin, v. 105, p. 1284–1296.

Hansen, J.W., Mason, S.J., Sun, L., and Tall, A., 2011, Review of seasonal climate forecasting for agriculture in sub-Saharan Africa: Experimental Agriculture, v. 47, no. 2, p. 205–240.

Head, M.J., and Gibbard, P.L., 2015, Early–Middle Pleistocene transitions: Linking terrestrial and marine realms: Quaternary International, v. 389, p. 7–46.

Hennissen, J.A., Head, M.J., De Schepper, S., and Groeneveld, J., 2015, Increased seasonality during the intensification of Northern Hemisphere glaciation at the Pliocene–Pleistocene boundary ~ 2.6 Ma: Quaternary Science Reviews, v. 129, p. 321–332.

Herbert, T.D., Ng, G., and Peterson, L.C., 2015, Evolution of Mediterranean sea surface temperatures 3.5–1.5Ma: Regional and hemispheric influence: Earth and Planetary Science Letters, v. 409, p. 307–318.

Hickson, J.A., Johnson, A.L., Heaton, T.H., and Balson, P.S., 1999, The shell of the Queen Scallop *Aequipecten opercularis* (L.) as a promising tool for palaeoenvironmental reconstruction: evidence and reasons for equilibrium stable-isotope incorporation: Palaeogeography, Palaeoclimatology, Palaeoecology, v. 154, no. 4, p. 325–337.

Holbourn, A.E., Henderson, A. S., and MacLeod, N., 2013, Atlas of Benthic Foraminifera: Wiley-Blackwell, p. 1–654.

Huyghe, D., Lartaud, F., Emmanuel, L., Merle, D., and Renard, M., 2015, Palaeogene climate evolution in the Paris Basin from oxygen stable isotope ($\delta^{18}O$) compositions of marine molluscs: Journal of the Geological Society, v. 172, no. 5, p. 576–587.

Iaccarino, S., 1985, Mediterranean Miocene and Pliocene planktic foraminifera. In Bolli H.H., Sanders, J.B., Perck-Nielsen K. (eds.), Plankton Stratigraphy, p. 283–314.

Iaccarino, S., Premoli Silva, I., Biolzi, M., Foresi, L.M., Lirer, F., Turco, E., and Petrizzo, M.R., 2007, Practical manual of Neogene Planktonic Foraminifera. International School on Planktonic Foraminifera, 6th course, Perugia 19-23 February 2007, University of Perugia, p. 1–181.

Ivany, L.C., Patterson, W.P., and Lohmann, K.C., 2000, Cooler winters as a possible cause of mass extinctions at the Eocene/Oligocene boundary: Nature, v. 407, p. 887–890.

Ivany, L.C., Lohmann, K.C., Hasiuk, F., Blacke, D.B., Glass, A., Aronson, R.B., and Moody, R.M., 2008. Eocene climate record of a high southern latitude continental shelf: Seymour Island, Antarctica: Geological Society of America Bulletin, v. 120, p. 659–678.

Ivany, L.C., and Runnegar, B., 2010, Early Permian seasonality from bivalve $\delta^{18}O$ and implications for the oxygen isotopic composition of seawater: Geology, v. 38, no. 11, p. 1027–1030.

Jiménez, A.P., Aguirre, J., and Rivas, P., 2009, Taxonomic study of scallops (Pectinidae: Mollusca, Bivalvia) from Pliocene deposits (Almería, SE Spain): Revista Española de Paleontología, v. 24 (1), p. 1–30.

Johnson, A.L.A., Hickson, J.A., Bird, A., Schöne, B.R., Balson, P.S., Heaton, T.H., and Williams, M., 2009, Comparative sclerochronology of modern and mid-Pliocene (c. 3.5 Ma)

Aequipecten opercularis (Mollusca, Bivalvia): an insight into past and future climate change in the north-east Atlantic region: Palaeogeography, Palaeoclimatology, Palaeoecology, v. 284 (3), p. 164–179.

Kennett, J.P., and Srinivasan, M.S., 1983, Neogene Planktonic Foraminifera: A Phylogenetic Atlas. Stroudsburg, PA (Hutchinson Ross).

Kim, S.-T., O'Neil, J.R., Hillaire-Marcel, C., and Mucci, A., 2007, Oxygen isotope fractionation between synthetic aragonite and water: influence of temperature and Mg^{2+} concentration: Geochimica et Cosmochimica Acta, v. 71, p. 4704–4715.

Kuhlemann, J., Rohling, E.J., Krumrei, I., Kubik, P., Ivy-Ochs, S., and Kucera, M., 2008, Regional synthesis of Mediterranean atmospheric circulation during the Last Glacial Maximum: Science, v. 321, p. 1338–1340.

Kukla, G., Collins, B.P., and Bender, M.L., 1979, Radiometric age of the *Arctica islandica* boundary in Italy: 2 my: Annales géologigues des Pays Helléniques, hors série, no. 2, p. 699–709.

Lamarck, J.B. de, 1819, Histoire naturelle des animaux sans vertèbres, A. Berlin, Paris, v. 6, 343 pp.

Lécuyer, C., Daux, V., Moissette, P., Cornée, J. J., Quillévéré, F., Koskeridou, E., Fourel, F., Martineau, F., and Reynard, B., 2012, Stable carbon and oxygen isotope compositions of invertebrate carbonate shells and the reconstruction of paleotemperatures and paleosalinities - A case study of the early Pleistocene of Rhodes, Greece: Palaeogeography, Palaeoclimatology, Palaeoecology, v. 350, p. 39–48.

Linnaeus, C., 1758, Systema Naturae per Regna tria naturae, secundum classes, ordines, genera, species cum characteribus, differentiis, synonymis, locis. Editio decima, reformata. Tomus 1, 824 pp. Laurentii Salvii, Holmiae.

Linnaeus, C., 1767, Systema Naturae per Regna tria naturae, secundum classes, ordines, genera, species cum characteribus, differentiis, synonymis, locis. Editio duodecima, reformata. Tomus 1, pars 2, 533–1327 pp. Laurentii Salvii, Holmiae.

Lisiecki, L.E., and Raymo, M.E., 2005, A Pliocene-Pleistocene stack of 57 globally distributed benthic $\delta^{18}O$ records: Paleoceanography, v. 20, no. 1, p. 522–533.

Lourens, L.J., Antonarakou, A., Hilgen, F.J., Van Hoof, A.A.M., Vergnaud-Grazzini, C., and Zachariasse, W.J., 1996, Evaluation of the Plio-Pleistocene astronomical timescale: Paleoceanography, v. 11 (4), p. 391.

Lourens, L.J., 2004, Revised tuning of Ocean Drilling Program Site 964 and KC01B (Mediterranean) and implications for the $\delta^{18}O$, tephra, calcareous nannofossil, and geomagnetic reversal chronologies of the past 1.1 Myr: Paleoceanography, v. 19, no. 3, PA3010, doi:10.1029/2003PA000997.

Lozano Francisco, M.C., Vera Pelaez, J.L., and Guerra Merchan, A., 1993, Arcoida (Mollusca, Bivalvia) del Plioceno de la provincia de Málaga, España: Treballs del Museu de Geologia de Barcelona, v. 3, p. 157–188.

Lutz, R.A., Goodsell, J.G., Mann, R., and Castagna, M., 1981, Experimental culture of the ocean quahog, *Arctica islandica*: Journal of World Aquaculture Society, v. 12, p. 196–205.

Maiorano, P., Capotondi, L. Ciaranfi, N., Girone, A., Lirer, F., Marino, M., Pelosi, N., Petrosino, P., and Piscitelli, A., 2010. Vrica-Crotone and Montalbano Jonioc sections: A potential unit-stratotype of the Calabrian Stage. Episodes, v. 33, no. 4, p. 218–233.

Malatesta, A., 1974, Malacofauna pliocenica umbra: Memoria per servire alla descrizione della Carta Geologica d'Italia, v. 13, p. 1–490.

Martínez-Garcia, A., Rosell-Melé, A., McClymont, E.L., Gersonde, R., and Haug, G.H., 2010, Subpolar link to the emergence of the modern Equatorial Pacific Cold Tongue: Science, v. 328, p. 1550–1553.

Martínez-García, B., Rodríguez-Lázaro, J., Pascual, A., and Mendicoa, J., 2015, The "Northern guests" and other palaeoclimatic ostracod proxies in the late Quaternary of the Basque Basin (S Bay of Biscay): Palaeogeography, Palaeoclimatology, Palaeoecology, v. 419, p. 100–114.

Martini, E., 1971, Standard Tertiary and Quaternary calcareous nannoplankton zonation, in Proceedings, International Conference Planktonic Microfossils, 2nd, Roma, Edizioni Tecnoscienza, v. 2, p. 739–785.

McConnaughey, T.A., and Gillikin, D.P., 2008, Carbon isotopes in mollusk shell carbonates: Geo-Marine Letters, v. 28 (5-6), p. 287–299.

Monechi, S., and Thierstein, H., 1985, Late Cretaceous-Eocene Nannofossil and Magnetostratigraphic Correlations Near Gubbio, Italy: Marine Micropaleontology, v. 9, p. 419–440.

Okada, H., and Bukry, D., 1980, Supplementary modification and introduction of code numbers to the low-latitude coccolith biostratigraphic zonation (Bukry 1973, 1975): Marine Micropaleontology, v. 5, p. 321–325.

Oliver, P.G., and Holmes, A.M., 2006, The Arcoidea (Mollusca: Bivalvia): a review of the current phenetic based systematics: Zoological Journal of the Linnean Society, v. 148, p. 237–251.

O'Neil, J.R., Clayton, R.N., and Mayeda, T.K., 1969, Oxygen isotope fractionation in divalent metal carbonates: Journal of Chemical Physics, v. 51, p. 5547–5558.

Paillard, D., 1996, Macintosh Program performs time-series analysis: Eos Transactions American Geophysical Union, v. 77, no. 39, p. 379–385.

Pelosio, G., and Raffi, S., 1977, Preliminary remarks on mollusc assemblages of the Stirone river Pleistocene series (Parma Province, Northern Italy): X INQUA Congress, Birmingham, p. 1–19.

Pierre, C., 1999, The oxygen and carbon isotope distribution in the Mediterranean water masses: Marine geology, v. 153 (1), p. 41–55.

Popp, B.N., Anderson, T.F., and Sandberg, P.A., 1986, Brachiopods as indicators of original isotopic compositions in some Paleozoic limestones: Geological Society of America, Bulletin, v. 97, p. 1262–1269.

Pross, J., and Klotz, S., 2002, Palaeotemperature calculations from the Praetiglian/Tiglian (Plio–Pleistocene) pollen record of Lieth, northern Germany: implications for the climatic evolution of NW Europe: Global and Planetary Change, v. 34, no. 3, p. 253–267.

Raffi, S., 1986, The significance of marine boreal molluscs in the Early Pleistocene faunas of the Mediterranean area, Palaeogeography, Palaeoclimatology, Palaeoecology, v. 52, p. 267–289.

Raffi, I., Backman, J., Rio, D., and Shackleton, N.J., 1993, Plio-Pleistocene nannofossil biostratigraphy and calibration to oxygen isotope stratigraphies from Deep Sea Drilling Project Site 607 and Ocean Drilling Program Site 677: Paleoceanography, v. 8, p. 387–408.

Ragaini, L., Cantalamessa, G., Di Celma, C., Didaskalou, P., Impiccini, R., Lori, P., Marino, M., Potetti, M. and Ragazzini, S., 2006, First Emilian record of the boreal-affinity bivalve *Portlandia impressa* Perri, 1975 from Montefiore dell'Aso (Marche, Italy): Bollettino della Società Paleontologica Italiana, v. 45, p. 227–234.

Raineri, G., 2007, Riserva naturale geologica del Piacenziano: appunti per un'escursione, Parchi e Riserve dell'Emilia-Romagna, 52 p.

Rohling, E. J., and Bigg, G. R., 1998, Paleosalinity and $\delta^{18}O$: a critical assessment: Journal of Geophysical Research: Oceans, v. 103(C1), p. 1307–1318.

Royer, C., Thébault, J., Chauvaud, L., and Olivier, F., 2013, Structural analysis and paleoenvironmental potential of dog cockle shells (*Glycymeris glycymeris*) in Brittany, northwest France: Palaeogeography, Palaeoclimatology, Palaeoecology: v. 373, p. 123–132.

Sarnthein, M., Bartoli, G., Prange, M., Schmittner, A., Schneider, B., Weinelt, M., Andersen, N., and Garbe-Schönberg, D., 2009, Mid-Pliocene shifts in ocean overturning circulation and the onset of Quaternary-style climates: Climate of the Past, v. 5, p. 269–283.

Schöne, B.R., 2013, *Arctica islandica* (Bivalvia): A unique paleoenvironmental archive of the northern North Atlantic Ocean: Global and Planetary Change, v. 111, p. 199–225.

Schöne, B.R., and Fiebig, J., 2009, Seasonality in the North Sea during the Allerød and Late Medieval Climate Optimum using bivalve sclerochronology: International Journal of Earth Sciences, v. 98 (1), p. 83–98.

Schöne, B.R., and Surge, D.M., 2012, Bivalve sclerochronology and geochemistry, in Selden, P.A., ed., Treatise of Invertebrate Paleontology, Treatise Online 46, Part N Revised, Mollusca (Bivalvia), v. 1, chapter 14, p. 1–24.

Schöne, B.R., Fiebig, J., Pfeiffer, M., Gleβ, R., Hickson, J., Johnson, A.L.A., Dreyer, W., and Oschmann, W., 2005, Climate records from a bivalved Methuselah (*Arctica islandica*, Mollusca; Iceland): Palaeogeography, Palaeoclimatology, Palaeoecology, v. 228 (1), p. 130–148.

Schrag, D.P., Adkins, J.F., McIntyre, K., Alexander, J.L., Hodell, D.A., Charles, C.D., and McManus, J.F., 2002, The oxygen isotopic composition of sea water during the Last Glacial Maximum: Quaternary Science Reviews, v. 21, p. 331–342.

Sosdian, S., and Rosenthal, Y., 2009, Deep-Sea Temperature and Ice Volume Changes Across the Pliocene-Pleistocene Climate Transitions: Science, v. 325, p. 306–310.

Steuber, T., Rauch, M., Masse, J. P., Graaf, J., and Malkoč, M., 2005, Low-latitude seasonality of Cretaceous temperatures in warm and cold episodes: Nature, v. 437, p. 1341–1344.

Suess, E., 1883–1888, Das Antlitz der Erde: Tempsky and Freytag (eds.), Prague (Czech Republic), Vienna (Austria) and Leipzig (Germany).

Tarutani, T., Clayton, R.N., and Mayeda, T., 1969, The effect of polymorphism and magnesium substitution on oxygen isotope fractionation between calcium carbonate and water: Geochimica et Cosmochimica Acta, v. 33, p. 987–996.

Thomas, R.D.K., 1976, Constraints of ligament growth, form and function on evolution in the Arcoida (Mollusca: Bivalvia): Paleobiology, v. 2, p. 64–83.

Thunell, R., Rio, D., Sprovieri, R., and Vergnaud-Grazzini, C., 1991, An overview of the post-Messinian paleoenvironmental history of the western Mediterranean: Paleoceanography, v. 6, p. 143–164.

Ulijaszek, S.J., and Strickland, S.S., 1993, Seasonality and human ecology: Cambridge University Press, 250 p.

Van Couvering, J.A., 1997, The Pleistocene boundary and the beginning of the Quaternary: Cambridge University Press, 296 p.

Wang, P., Tian, J., and Lourens, L.J., 2010, Obscuring of long eccentricity cyclicity in Pleistocene oceanic carbon isotope records: Earth and Planetary Science Letters, v. 290, no. 3–4, p. 319-330.

Witbaard, R., 1997, Tree of the sea. The use of internal growth lines in the shell of *Arctica islandica* (Bivalvia, Mollusca) for the retrospective assessment of marine environmental change. PhD thesis Rijksuniversiteit Groningen (157 pp.).

Zavatarelli, M., Raicich, F., Bregant, D., Russo, A., and Artegiani, A., 1998, Climatological biogeochemical characteristics of the Adriatic Sea: Journal of Marine Systems, v. 18, no. 1, p. 227–263.

Zhou, G.T., and Zheng, Y.F., 2003, An experimental study of oxygen isotope fractionation between inorganically precipitated aragonite and water at low temperatures, Geochimica et Cosmochimica Acta, v. 67, p. 387–399.

FIGURE CAPTIONS

Figure 1. Geological map of northern Italy showing the study area.

Figure 2. Biostratigraphy and stack correlation. A) LR04 stack (Lisiecki and Raymo, 2005) based on benthic foraminifera. B) Mediterranean stack (Medstack) based on planktonic foraminifera (Lourens, 2004; Wang et al., 2010). C) Mean $\delta^{18}O_{wh}$ curve obtained from whole shells oxygen isotope analyses performed on species of *Glycymeris*, *Aequipecten* and *Arctica*; in red are tie-points obtained from nannofossil biostratigraphy; in grey are added pointers. Triangles represent the position of the shells sclerochemically analyzed: *Glycymeris* in yellow, *Arctica* in pink. D) Calcareous nannofossil (following Backman et al., 2012) and foraminifera

biostratigraphy of the Arda section with the most important bioevents. E) Stratigraphic log of the section; base of the section: 44°51’18.52’’N; 9°52’26.7’’E. The section starts 200 m downstream of the bridge located at the entrance to the town of Castell’Arquato.

Figure 3. Calcareous nannofossil bio-horizons and zones identified in the Arda section (following Backman et al., 2012). Total abundance of nannofossils (expressed as number of specimens/field of view) and abundance (in %) of reworked Lower Cretaceous species, Upper Cretaceous species, Paleogene and Pliocene species and of *in situ Gephyrocapsa* divided into “small”, “medium” and “large”.

Figure 4. Calcareous nannofossil micrographs (XPL, cross-polarized light) of the most common taxa identified in the Arda section. The scale bar represents 5 μm where not differently specified: (1) *Gephyrocapsa* “small”, Sample ACN79, 79.95 m. (2) *Gephyrocapsa* “small”, Sample ACN79, 79.95 m. (3) *Gephyrocapsa* “medium”, Sample ACN101, 168 m. (4) *Gephyrocapsa* “medium”, Sample ACN101, 168 m. (5) *Gephyrocapsa* “large” Sample ACN203, 180 m. (6) *Syracosphaera pulchra*, Sample ACN79, 79.95 m. (7) *Helicosphaera sellii*, Sample ACN79, 79.95 m. (8) *Helicosphaera sellii*, Sample ACN79, 79.95 m. (9) *Calcidiscus leptoporus*, Sample ACN79, 79.95 m. (10) *Coccolithus pelagicus*, Sample ACN79, 79.95 m. (11) *Sphenolithus* sp., Sample ACN79, 79.9 5m. (12) *Pseudoemiliania lacunosa*, Sample ACN79, 79.95 m. (13) *Reticulofenestra lockeri*, Sample ACN201, 176 m. (14) *Pontosphaera multipora*, Sample ACN203, 180 m. (15) *Zeugrhabdotus bicrescenticus*, Sample ACN203, 180 m. (16) Ascidian spicules, Sample ACN34, 48 m. (17) *Rhabdosphaera clavigera*, Sample ACN36, 50 m. (18) *Prediscosphaera columnata*, Sample ACN79, 79.95 m. (19) *Nannoconus steinmannii* Sample

ACN203, 180 m. (20) *Micula staurofora* Sample ACN79, 79.95 m. (21) *Discoaster* sp. Sample 1-52G. (22) *Discoaster* sp. Sample 1-52G. Scanning Electron Microscope micrographs: (23) *Gephyrocapsa* "small", Sample ACN84, 127 m. (24) *Gephyrocapsa* "small", Sample ACN84, 127 m. (25) *Syracosphaera* sp., Sample ACN224, 227 m.

Figure 5. SEM images of some species of foraminifera identified in the Arda section. (1a–c) - *Globigerina cariacoensis* (a umbilical view, b lateral view, c spiral view; scale bar 200 μm), Sample ACF28, 37.05 m. (2a–c) *Globigerina bulloides* (a umbilical view, b lateral view, c spiral view; scale bar 100 μm), Sample ACF220, 221 m. (3a–d) *Globigerinoides obliquus extremus* (a umbilical view, b lateral view, c spiral view; scale bar 200 μm), (d magnified view of the aperture with spines preserved; scale bar 20 μm), Sample ACF52, 63 m. (4a–c) *Neogloboquadrina pachyderma* left-coiling (a umbilical view, b lateral view, c spiral view; scale bar 100 μm), Sample AC34, 48 m. (5a–c) *Hyalinea balthica* (a, c side views, b lateral view; scale bar 100 μm), Sample ACF220, 221 m. (6a–d) *Globigerinoides elongatus* (a umbilical view, b lateral view, c spiral view; scale bar 100 μm), (6d magnified view of the aperture with spines preserved, scale bar 10 μm), Sample ACF34, 48 m. (7a–b) *Uvigerina mediterranea* (a lateral view, b apertural view; scale bar 100 μm), Sample ACF28, 37.05 m. (8a–b) *Uvigerina bradyana* (a, b lateral views; scale bar 100 μm), Sample ACF28, 37.05 m. (9a–b) *Bulimina etnea* (a, b lateral views; scale bar 200 μm), Sample ACF214, 206 m. (10a–b) *Bulimina elegans marginata* (a, b lateral views; scale bar 200 μm), Sample ACF220, 221 m.

Figure 6. Legend: CF: crossed foliated; CCF: complex crossed foliated; CL: crossed lamellar; CCL: complex crossed lamellar; GL: growth line; IL: inner layer; ISP: irregular simple

prismatic; ML: middle layer; OL: outer layer; OS: outer surface; Pm: pallial myostracum; SC: sparry calcite. F: fossil specimen; R: recent specimen. For *Glycymeris* shells see also Crippa, 2013.

(A) Cone complex crossed lamellar inner layer. *Glycymeris insubrica* (ACG98-3). (B) Irregular complex crossed lamellar inner layer crossed by growth lines made of irregular simple prisms. *Glycymeris glycymeris* (AG2). (C) Prismatic pallial myostracum. *Glycymeris insubrica* (ACG59-1). (D) First order lamellae of the outer layer crossed by a growth line. *Glycymeris glycymeris* (AG1). (E) Well preserved crossed lamellae of the outer layer: first, second and third order elements are clearly observable. *Glycymeris glycymeris* (ACG14-4). (F) Regular foliated fabric of the inner layer. *Aequipecten opercularis* (ACG70-3). (G) Crossed foliated fabric of the inner layer. *Aequipecten opercularis* (ACG90-7). (H) Regular foliated outer layer, irregular simple prismatic pallial myostracum and, crossed lamellar and irregular simple prismatic pallial myostracum. *Aequipecten opercularis* (ACG235-4). (I) Section showing the complex organization of the shell. The outer and inner layers are composed of a regular foliated fabric. The middle layer shows a double pattern of crossed lamellae (simple and complex) separated by a thin layer of irregular simple prisms; inward there is a thick layer of irregular simple prisms. *Aequipecten opercularis* (ACG100-2). (J) Sparry calcite replacing the aragonitic middle layer in an altered shell. *Aequipecten scabrella* (ACG6-8). (K) Middle and outer layer of an altered shell. Note the sparry calcite replacing the aragonitic crossed lamellae. *Aequipecten scabrella* (ACG6-8). (L) Homogeneous outer layer. *Arctica islandica* (ACG228-1). (M) Homogeneous outer layer. *Arctica islandica* (AG3). (N) Fine complex crossed lamellar inner layer crossed by an irregular prismatic growth line. *Arctica islandica* (ACG86-4). (O) Fine complex crossed lamellar inner layer crossed by an irregular prismatic growth line. *Arctica islandica* (AG3).

Figure 7. Transmitted light thin-section (1) and cathodoluminescence (2) photomicrographs. (A1-2) Non-luminescent shell of *Glycymeris inflata* (ACG14-25); (B1-2) Non-luminescent shell of *Glycymeris glycymeris* (ACG27bis-8); (C1-2) Non-luminescent shell of *Aequipecten opercularis* (ACG81-2); (D1-2) Non-luminescent shell of *Aequipecten opercularis* (ACG34-1); note the luminescence of the matrix due to Mn-enriched diagenetic cements and recrystallized allochems; (E1-2) Non-luminescent shell of *Arctica islandica* (ACG78-1); (F1-2) Non-luminescent shell of *Arctica islandica* (ACG254-4).

Figure 8. $\delta^{18}O_{sh}$ (violet) and $\delta^{13}C_{sh}$ (green) data from *Arctica islandica* shells from the base to the top of the section. The position of the growth lines is represented by vertical grey bands. LD: living depth (hypothesized on the basis of the sedimentary structures and the faunal associations present in the corresponding bed). FZ: Foraminifera Zones, CNZ: Calcareous Nannofossil Zones.

Figure 9. $\delta^{18}O_{sh}$ (violet) and $\delta^{13}C_{sh}$ (green) data from *Glycymeris* shells from the base to the top of the section. The position of the growth lines is represented by vertical grey bands. LD: living depth (hypothesized on the basis of the sedimentary structures and the faunal associations present in the corresponding bed). FZ: Foraminifera Zones, CNZ: Calcareous Nannofossil Zones.

Table 1. $\delta^{18}O_{sh}$ from the ten shells of *A. islandica* (A) and of *G. inflata* and *G. insubrica* (B) analyzed for isotope sclerochemistry. $\delta^{18}O_{sh\ max\text{-}excursion}$: difference between the maximum ($\delta^{18}O_{sh\text{-}max}$) and minimum ($\delta^{18}O_{sh\text{-}min}$) oxygen isotope values of the larger amplitude cycle, corresponding to the maximum seasonal variation occurring in that specimen (approach 1 in the

text). $\delta^{18}O_{sh\ mean\text{-}excursion}$: difference between the mean of all defined maxima ($\delta^{18}O_{sh\ mean\text{-}max}$) and minima ($\delta^{18}O_{sh\ mean\text{-}min}$) from each annual increment in every shell, corresponding to the mean seasonal excursion (approach 2 in the text). For both approaches we calculated the corresponding maximum (T_{max}, $T_{mean\text{-}max}$) and minimum (T_{min}, $T_{mean\text{-}min}$) paleotemperatures and paleotemperature excursions ($T_{max\text{-}excusion}$, $T_{mean\text{-}excursion}$) using the modified equation of Grossman and Ku (1986); the value of seawater $\delta^{18}O_{sw}$ (V-SMOW) used in each stratigraphic bed has been assumed as described in the text. The shell position in the section is reported in meters from the base. AGI: number of annual growth increments sampled in each shell. MTS: average of the total oxygen isotope values in each shell.

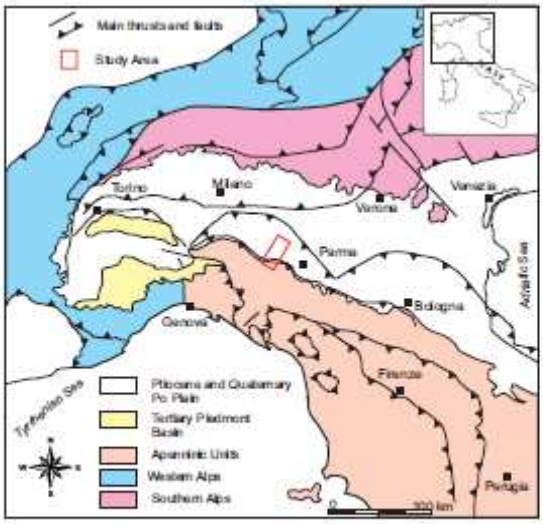

Figure 1

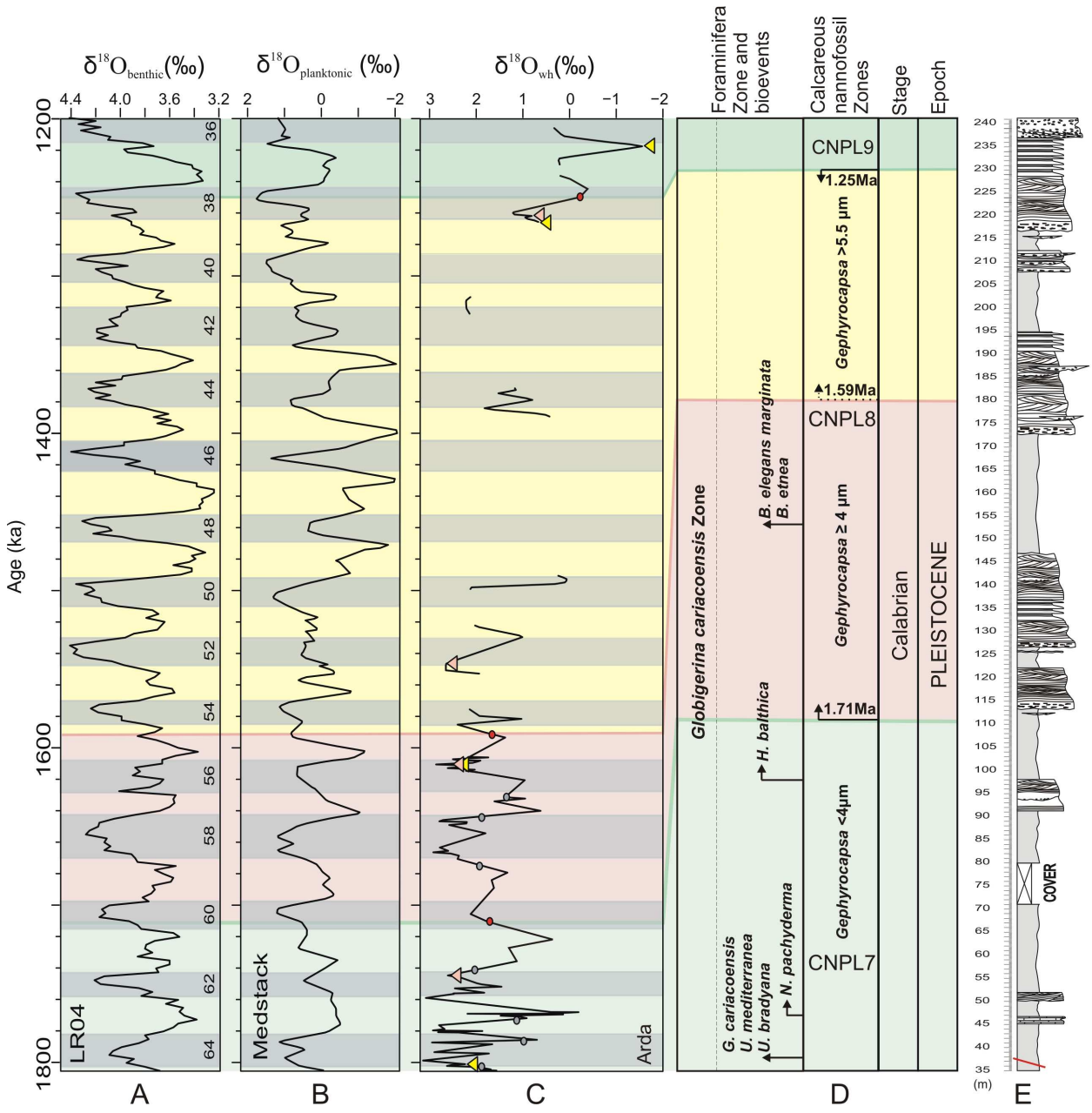

Figure 2

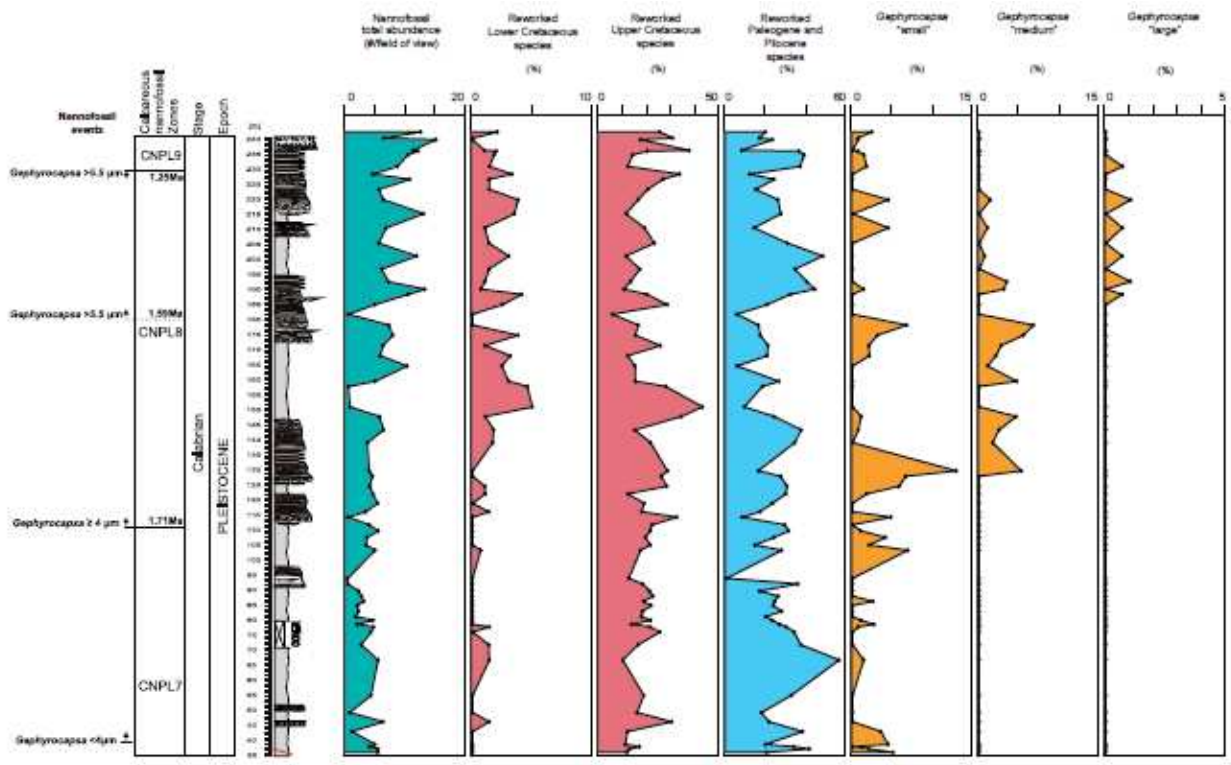

Figure 3

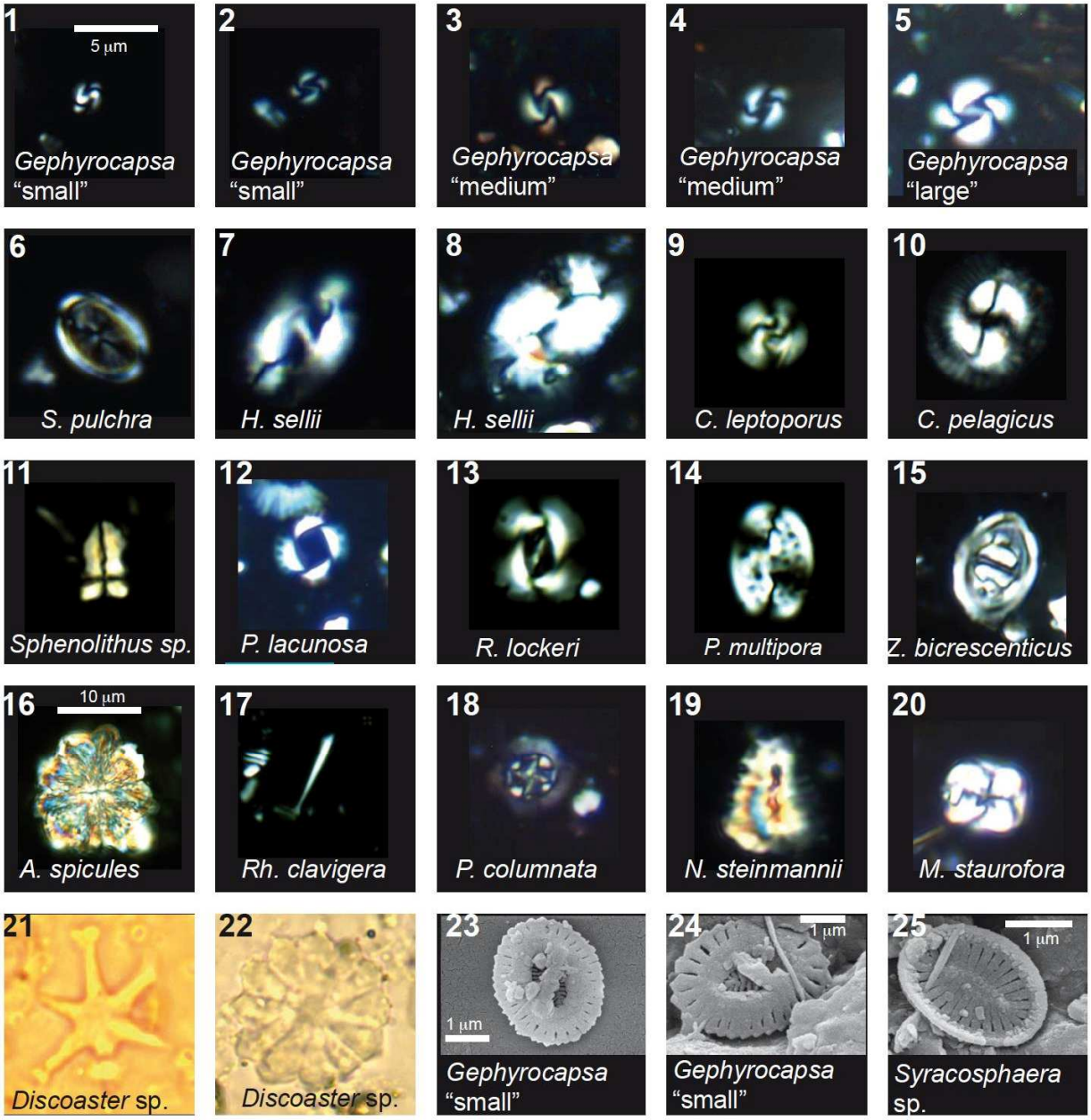

Figure 4

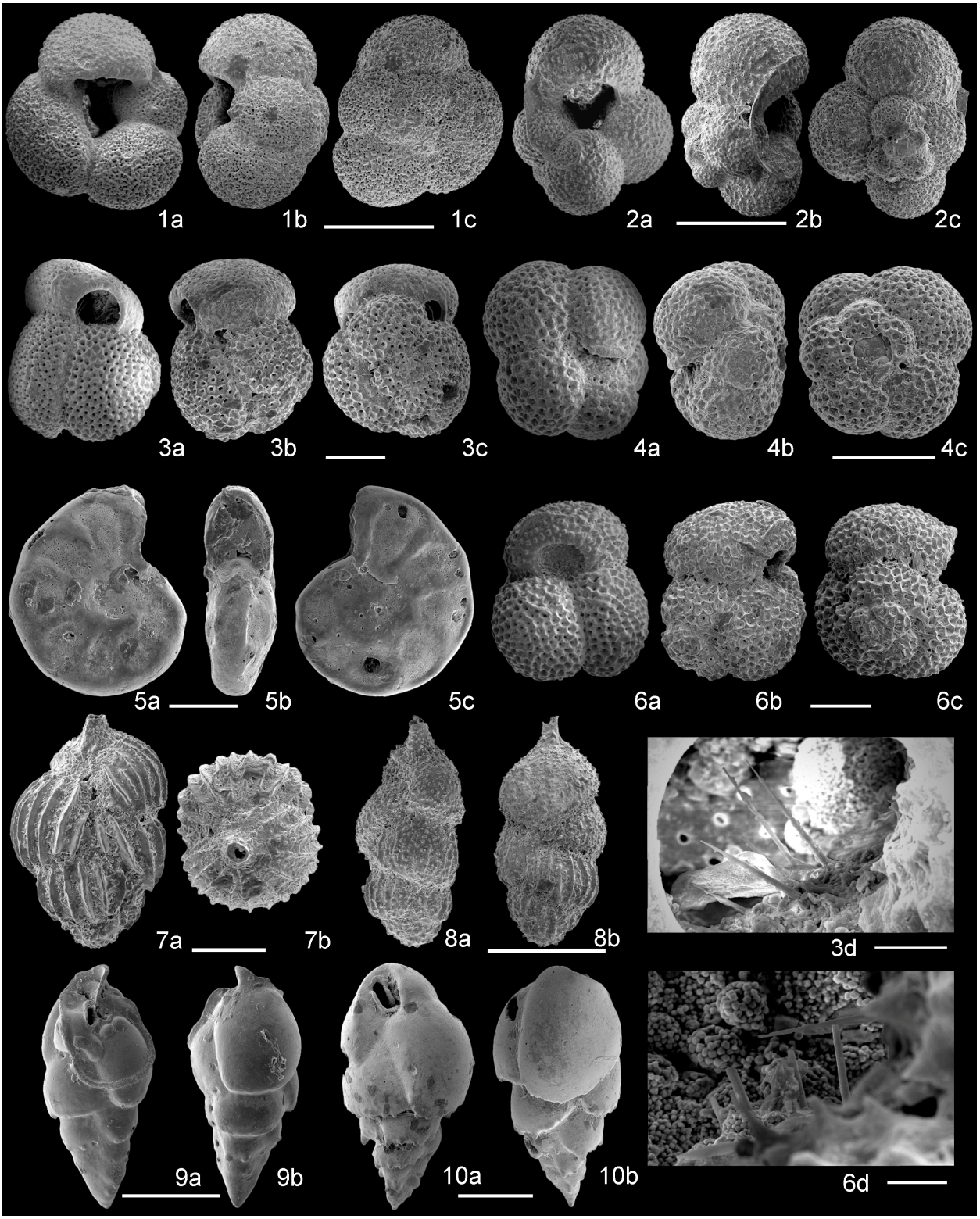

Figure 5

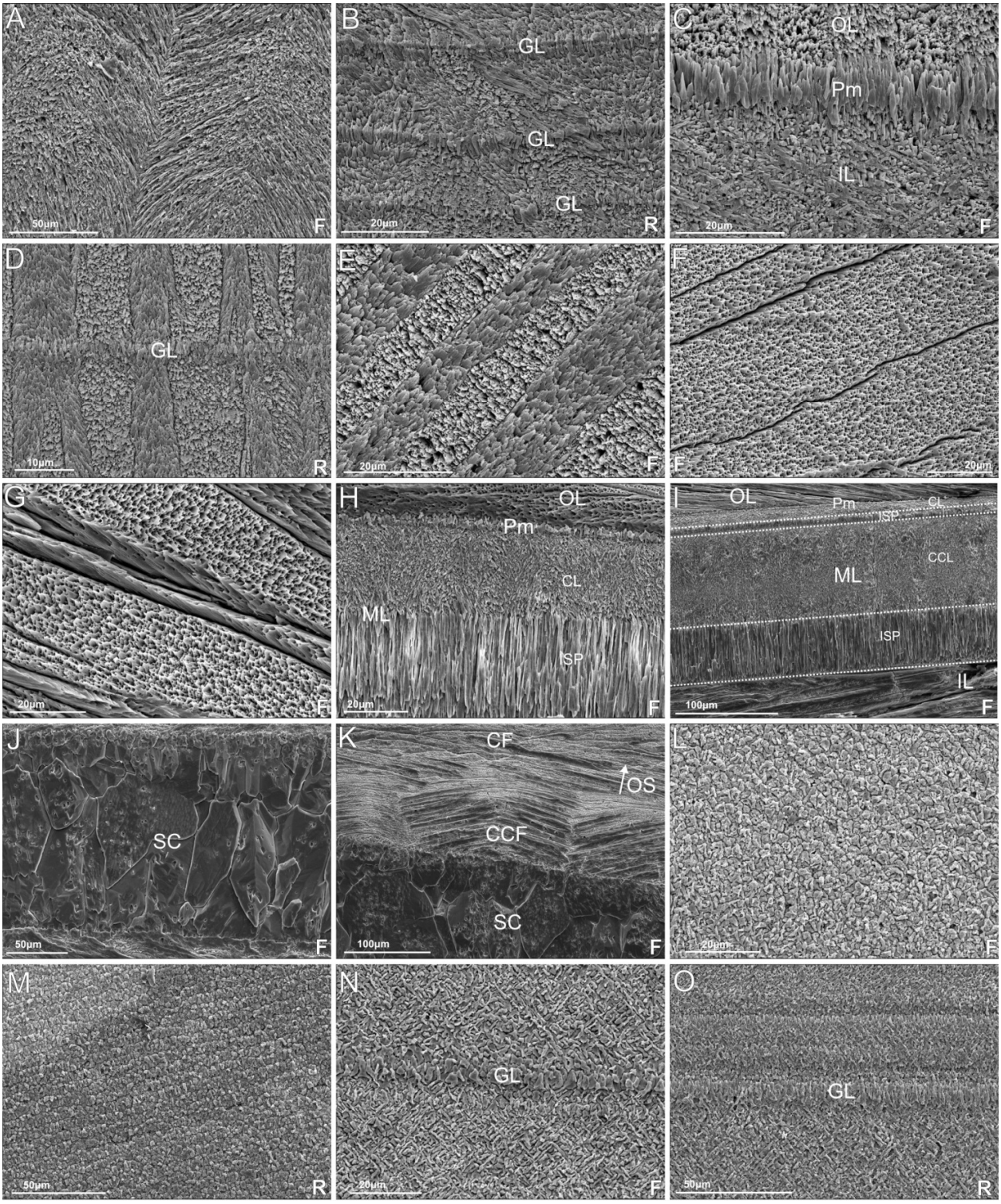

Figure 6

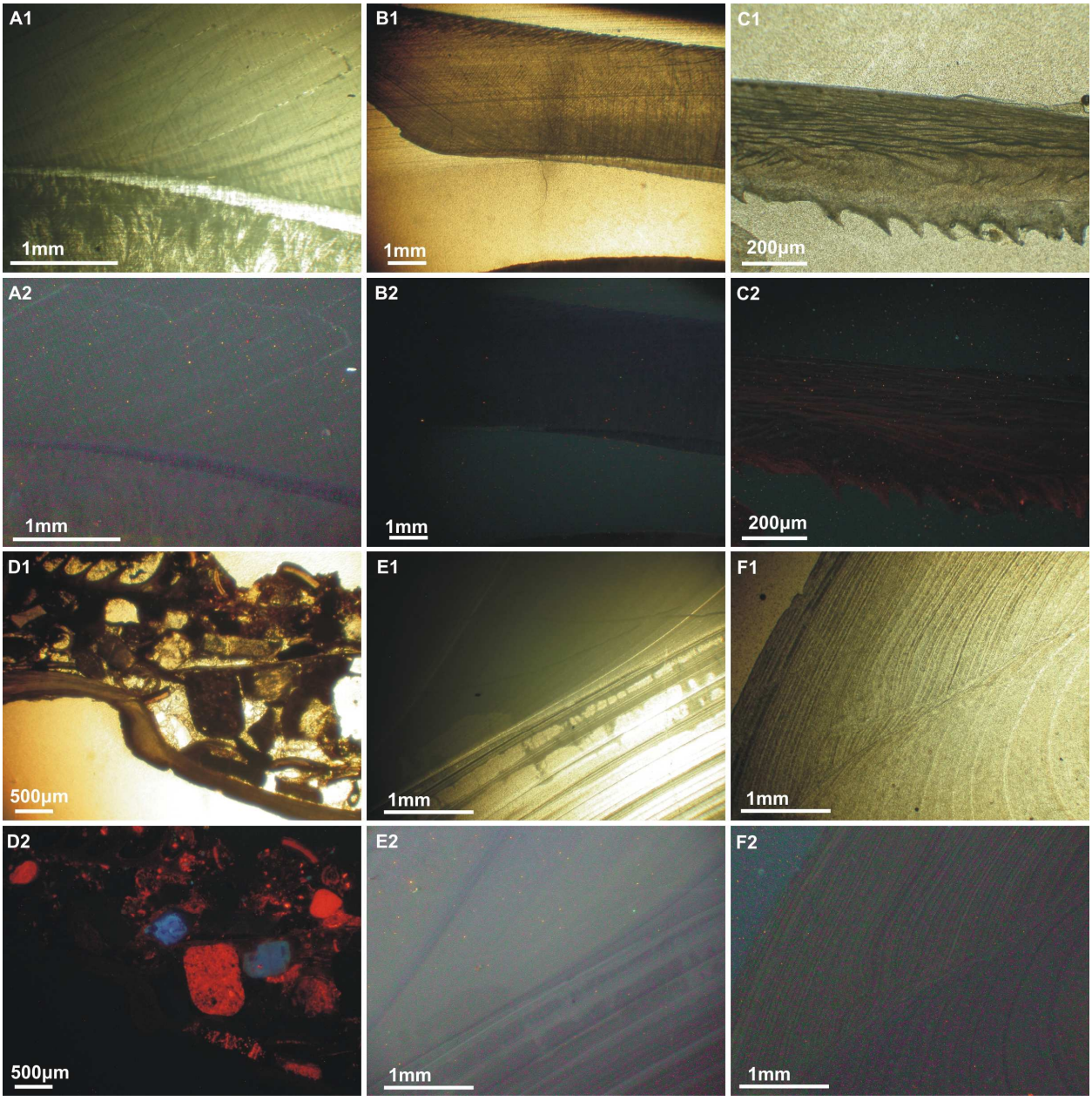

Figure 7

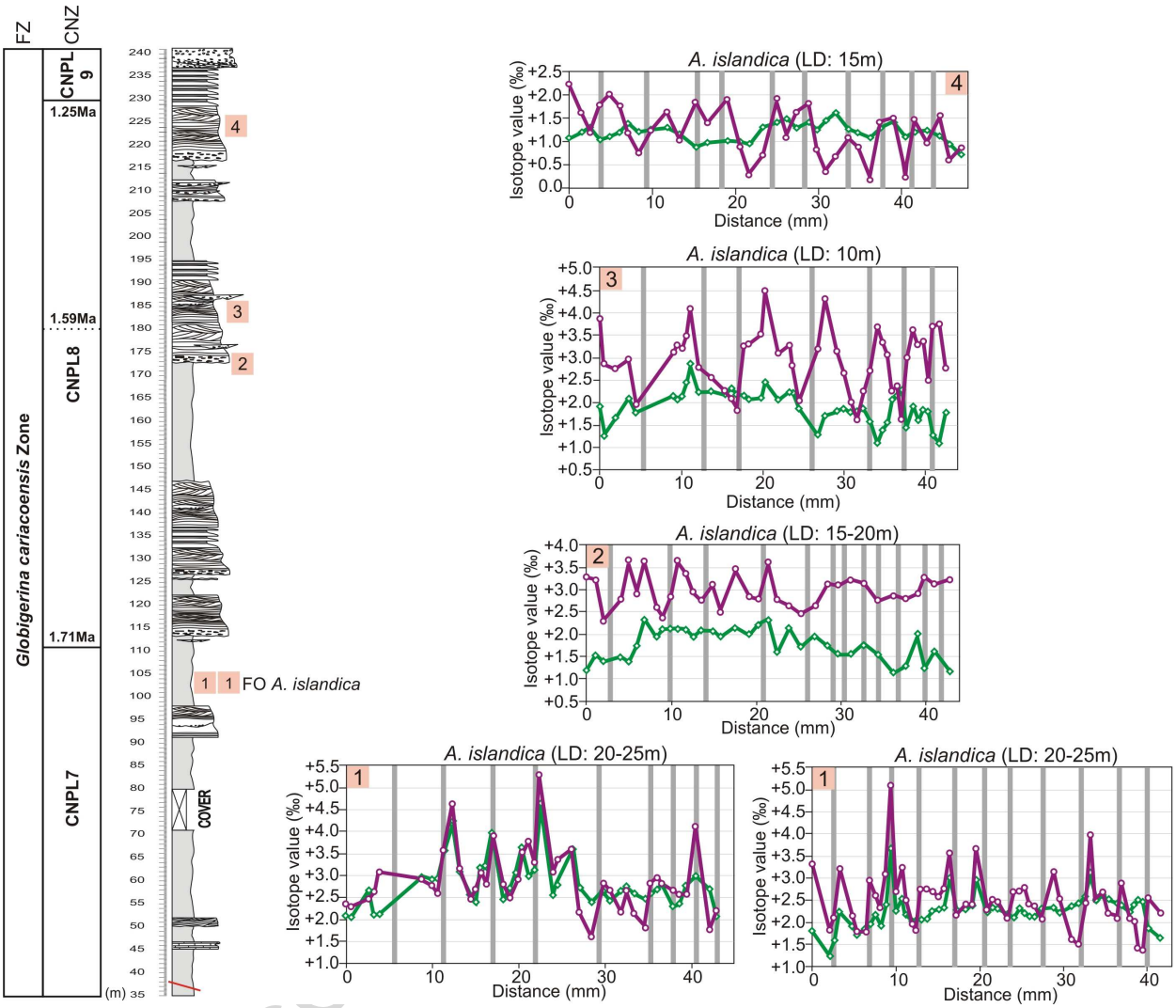

Figure 8

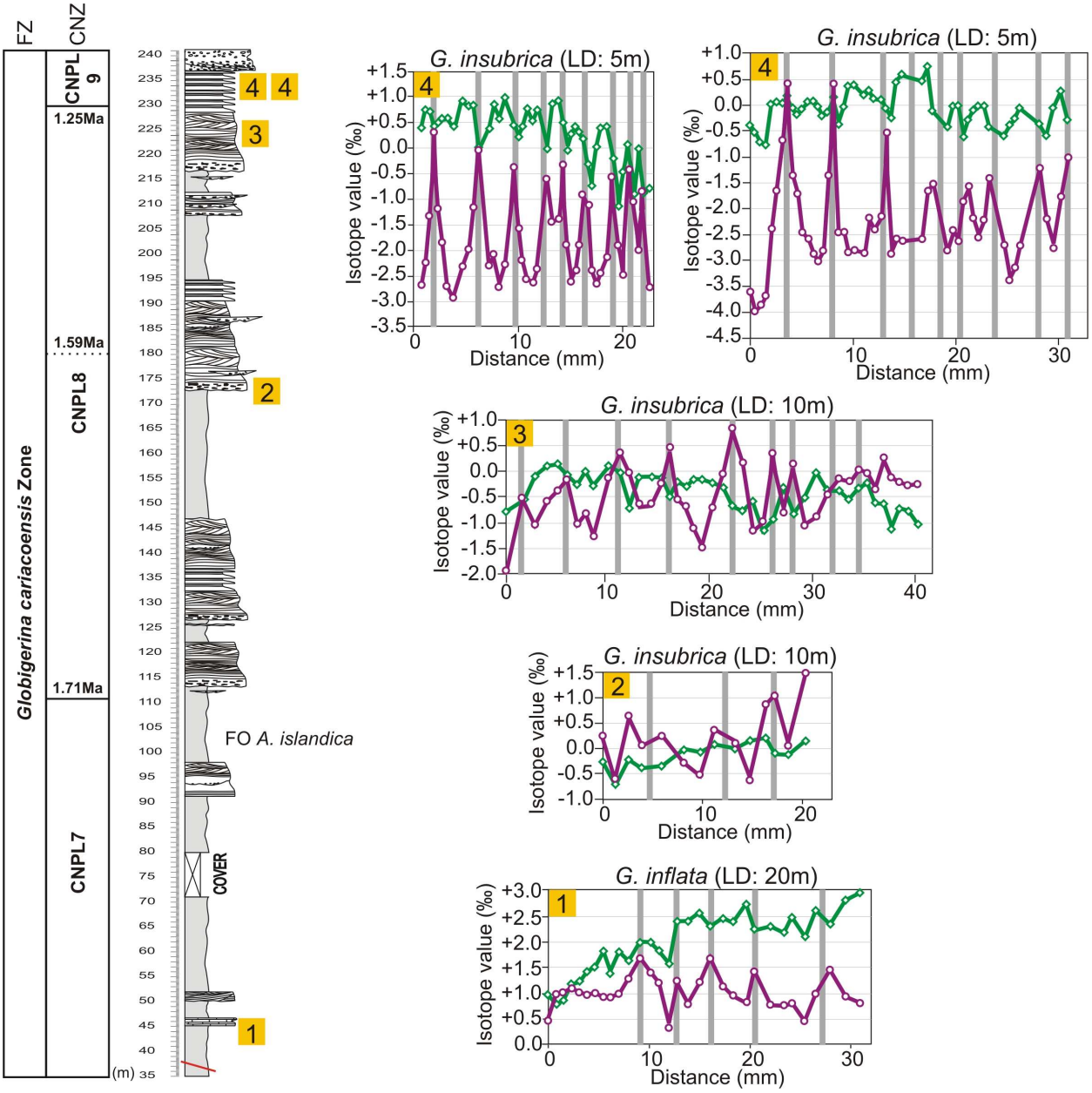

Figure 9

FIGURE CAPTIONS

Figure 1. Geological map of northern Italy showing the study area.

Figure 2. Biostratigraphy and stack correlation. A) LR04 stack (Lisiecki and Raymo, 2005) based on benthic foraminifera. B) Mediterranean stack (Medstack) based on planktonic foraminifera (Lourens, 2004; Wang et al., 2010). C) Mean $\delta^{18}O_{wh}$ curve obtained from whole shells oxygen isotope analyses performed on species of *Glycymeris*, *Aequipecten* and *Arctica*; in red are tie-points obtained from nannofossil biostratigraphy; in grey are added pointers. Triangles represent the position of the shells sclerochemically analyzed: *Glycymeris* in yellow, *Arctica* in pink. D) Calcareous nannofossil (following Backman et al., 2012) and foraminifera biostratigraphy of the Arda section with the most important bioevents. E) Stratigraphic log of the section; base of the section: 44°51'18.52''N; 9°52'26.7''E. The section starts 200 m downstream of the bridge located at the entrance to the town of Castell'Arquato.

Figure 3. Calcareous nannofossil bio-horizons and zones identified in the Arda section (following Backman et al., 2012). Total abundance of nannofossils (expressed as number of specimens/field of view) and abundance (in %) of reworked Lower Cretaceous species, Upper Cretaceous species, Paleogene and Pliocene species and of *in situ Gephyrocapsa* divided into "small", "medium" and "large".

Figure 4. Calcareous nannofossil micrographs (XPL, cross-polarized light) of the most common taxa identified in the Arda section. The scale bar represents 5 μm where not differently specified: (1) *Gephyrocapsa* "small", Sample ACN79, 79.95 m. (2) *Gephyrocapsa* "small", Sample

ACN79, 79.95 m. (3) *Gephyrocapsa* "medium", Sample ACN101, 168 m. (4) *Gephyrocapsa* "medium", Sample ACN101, 168 m. (5) *Gephyrocapsa* "large" Sample ACN203, 180 m. (6) *Syracosphaera pulchra*, Sample ACN79, 79.95 m. (7) *Helicosphaera sellii*, Sample ACN79, 79.95 m. (8) *Helicosphaera sellii*, Sample ACN79, 79.95 m. (9) *Calcidiscus leptoporus*, Sample ACN79, 79.95 m. (10) *Coccolithus pelagicus*, Sample ACN79, 79.95 m. (11) *Sphenolithus* sp., Sample ACN79, 79.9 5m. (12) *Pseudoemiliania lacunosa*, Sample ACN79, 79.95 m. (13) *Reticulofenestra lockeri*, Sample ACN201, 176 m. (14) *Pontosphaera multipora*, Sample ACN203, 180 m. (15) *Zeugrhabdotus bicrescenticus*, Sample ACN203, 180 m. (16) Ascidian spicules, Sample ACN34, 48 m. (17) *Rhabdosphaera clavigera*, Sample ACN36, 50 m. (18) *Prediscosphaera columnata*, Sample ACN79, 79.95 m. (19) *Nannoconus steinmannii* Sample ACN203, 180 m. (20) *Micula staurofora* Sample ACN79, 79.95 m. (21) *Discoaster* sp. Sample 1-52G. (22) *Discoaster* sp. Sample 1-52G. Scanning Electron Microscope micrographs: (23) *Gephyrocapsa* "small", Sample ACN84, 127 m. (24) *Gephyrocapsa* "small", Sample ACN84, 127 m. (25) *Syracosphaera* sp., Sample ACN224, 227 m.

Figure 5. SEM images of some species of foraminifera identified in the Arda section. (1a–c) - *Globigerina cariacoensis* (a umbilical view, b lateral view, c spiral view; scale bar 200 μm), Sample ACF 28, 37.05 m. (2a–c) *Globigerina bulloides* (a umbilical view, b lateral view, c spiral view; scale bar 100 μm), Sample ACF 220, 221 m. (3a–d) *Globigerinoides obliquus extremus* (a umbilical view, b lateral view, c spiral view; scale bar 200 μm), (d magnified view of the aperture with spines preserved; scale bar 20 μm), Sample ACF 52, 63 m. (4a–c) *Neogloboquadrina pachyderma* left-coiling (a umbilical view, b lateral view, c spiral view; scale bar 100 μm), Sample ACF 34, 48 m. (5a–c) *Hyalinea balthica* (a, c side views, b lateral view;

scale bar 100 μm), Sample ACF 220, 221 m. (6a–d) *Globigerinoides elongatus* (a umbilical view, b lateral view, c spiral view; scale bar 100 μm), (6d magnified view of the aperture with spines preserved, scale bar 10 μm), Sample ACF 34, 48 m. (7a–b) *Uvigerina mediterranea* (a lateral view, b apertural view; scale bar 100 μm), Sample ACF 28, 37.05 m. (8a–b) *Uvigerina bradyana* (a, b lateral views; scale bar 100 μm), Sample ACF 28, 37.05 m. (9a–b) *Bulimina etnea* (a, b lateral views; scale bar 200 μm), Sample ACF 214, 206 m. (10a–b) *Bulimina elegans marginata* (a, b lateral views; scale bar 200 μm), Sample ACF 220, 221 m.

Figure 6. Legend: CF: crossed foliated; CCF: complex crossed foliated; CL: crossed lamellar; CCL: complex crossed lamellar; GL: growth line; IL: inner layer; ISP: irregular simple prismatic; ML: middle layer; OL: outer layer; OS: outer surface; Pm: pallial myostracum; SC: sparry calcite. F: fossil specimen; R: recent specimen. For *Glycymeris* shells see also Crippa, 2013.

(A) Cone complex crossed lamellar inner layer. *Glycymeris insubrica* (ACG98-3). (B) Irregular complex crossed lamellar inner layer crossed by growth lines made of irregular simple prisms. *Glycymeris glycymeris* (AG2). (C) Prismatic pallial myostracum. *Glycymeris insubrica* (ACG59-1). (D) First order lamellae of the outer layer crossed by a growth line. *Glycymeris glycymeris* (AG1). (E) Well preserved crossed lamellae of the outer layer: first, second and third order elements are clearly observable. *Glycymeris glycymeris* (ACG14-4). (F) Regular foliated fabric of the inner layer. *Aequipecten opercularis* (ACG70-3). (G) Crossed foliated fabric of the inner layer. *Aequipecten opercularis* (ACG90-7). (H) Regular foliated outer layer, irregular simple prismatic pallial myostracum and, crossed lamellar and irregular simple prismatic pallial myostracum. *Aequipecten opercularis* (ACG235-4). (I) Section showing the complex

organization of the shell. The outer and inner layers are composed of a regular foliated fabric. The middle layer shows a double pattern of crossed lamellae (simple and complex) separated by a thin layer of irregular simple prisms; inward there is a thick layer of irregular simple prisms. *Aequipecten opercularis* (ACG100-2). (J) Sparry calcite replacing the aragonitic middle layer in an altered shell. *Aequipecten scabrella* (ACG6-8). (K) Middle and outer layer of an altered shell. Note the sparry calcite replacing the aragonitic crossed lamellae. *Aequipecten scabrella* (ACG6-8). (L) Homogeneous outer layer. *Arctica islandica* (ACG228-1). (M) Homogeneous outer layer. *Arctica islandica* (AG3). (N) Fine complex crossed lamellar inner layer crossed by an irregular prismatic growth line. *Arctica islandica* (ACG86-4). (O) Fine complex crossed lamellar inner layer crossed by an irregular prismatic growth line. *Arctica islandica* (AG3).

Figure 7. Transmitted light thin-section (1) and cathodoluminescence (2) photomicrographs. (A1-2) Non-luminescent shell of *Glycymeris inflata* (ACG14-25); (B1-2) Non-luminescent shell of *Glycymeris glycymeris* (ACG27bis-8); (C1-2) Non-luminescent shell of *Aequipecten opercularis* (ACG81-2); (D1-2) Non-luminescent shell of *Aequipecten opercularis* (ACG34-1); note the luminescence of the matrix due to Mn-enriched diagenetic cements and recrystallized allochems; (E1-2) Non-luminescent shell of *Arctica islandica* (ACG78-1); (F1-2) Non-luminescent shell of *Arctica islandica* (ACG254-4).

Figure 8. $\delta^{18}O_{sh}$ (violet) and $\delta^{13}C_{sh}$ (green) data from *Arctica islandica* shells from the base to the top of the section. The position of the growth lines is represented by vertical grey bands. LD: living depth (hypothesized on the basis of the sedimentary structures and the faunal associations present in the corresponding bed). FZ: Foraminifera Zones, CNZ: Calcareous Nannofossil Zones.

Figure 9. $\delta^{18}O_{sh}$ (violet) and $\delta^{13}C_{sh}$ (green) data from *Glycymeris* shells from the base to the top of the section. The position of the growth lines is represented by vertical grey bands. LD: living depth (hypothesized on the basis of the sedimentary structures and the faunal associations present in the corresponding bed). FZ: Foraminifera Zones, CNZ: Calcareous Nannofossil Zones.

TABLE CAPTION

Table 1. $\delta^{18}O_{sh}$ from the ten shells of *A. islandica* (A) and of *G. inflata* and *G. insubrica* (B) analyzed for isotope sclerochemistry. $\delta^{18}O_{sh\ max\text{-}excursion}$: difference between the maximum ($\delta^{18}O_{sh\text{-}max}$) and minimum ($\delta^{18}O_{sh\text{-}min}$) oxygen isotope values of the larger amplitude cycle, corresponding to the maximum seasonal variation occurring in that specimen (approach 1 in the text). $\delta^{18}O_{sh\ mean\text{-}excursion}$: difference between the mean of all defined maxima ($\delta^{18}O_{sh\ mean\text{-}max}$) and minima ($\delta^{18}O_{sh\ mean\text{-}min}$) from each annual increment in every shell, corresponding to the mean seasonal excursion (approach 2 in the text). For both approaches we calculated the corresponding maximum (T_{max}, $T_{mean\text{-}max}$) and minimum (T_{min}, $T_{mean\text{-}min}$) paleotemperatures and paleotemperature excursions ($T_{max\text{-}excusion}$, $T_{mean\text{-}excursion}$) using the modified equation of Grossman and Ku (1986); the value of seawater $\delta^{18}O_{sw}$ (V-SMOW) used in each stratigraphic bed has been assumed as described in the text. The shell position in the section is reported in meters from the base. AGI: number of annual growth increments sampled in each shell. MTS: average of the total oxygen isotope values in each shell.

Table 1

A

Species	Sample number	Position	$\delta^{18}O_{sh\text{-}min}$	T_{max}	$\delta^{18}O_{sh\text{-}max}$	T_{min}	$\delta^{18}O_{sh\ max\text{-}excursion}$	$T_{max\text{-}excursion}$
A. islandica	ACG254-1	224 m	+0.3 ‰	20.3 °C	+1.9 ‰	13.4 °C	1.6 ‰	6.9 °C
A. islandica	ACG215-5	185.70 m	+1.6 ‰	16.8 °C	+4.3 ‰	5.1 °C	2.7 ‰	11.7 °C
A. islandica	ACG200-13	174 m	+2.4 ‰	12.5 °C	+3.6 ‰	7.3 °C	1.2 ‰	5.2 °C
A. islandica	ACG78-7	103.70 m	+1.8 ‰	16.0 °C	+5.1 ‰	1.6 °C	3.3 ‰	14.4 °C
A. islandica	ACG78-1	103.70 m	+1.6 ‰	16.8 °C	+5.3 ‰	0.8 °C	3.7 ‰	16.0 °C

Species	Sample number	Position	$\delta^{18}O_{sh\ mean\text{-}min}$	$T_{mean\text{-}max}$	$\delta^{18}O_{sh\ mean\text{-}max}$	$T_{mean\text{-}min}$	$\delta^{18}O_{sh\ mean\text{-}excursion}$	$T_{mean\text{-}excursion}$
A. islandica	ACG254-1	224 m	+0.6 ‰	19.0 °C	+1.6 ‰	14.7 °C	1.0 ‰	4.3 °C
A. islandica	ACG215-5	185.70 m	+2.1 ‰	14.7 °C	+4.0 ‰	6.4 °C	1.9 ‰	8.3 °C
A. islandica	ACG200-13	174 m	+2.5 ‰	12.0 °C	+3.5 ‰	7.7 °C	1.0 ‰	4.3 °C
A. islandica	ACG78-7	103.70 m	+1.9 ‰	15.5 °C	+3.9 ‰	6.8 °C	2.0 ‰	8.7 °C
A. islandica	ACG78-1	103.70 m	+2.0 ‰	15.1 °C	+4.5 ‰	4.2 °C	2.5 ‰	10.9 °C

Species	Sample number	Position	MTS	V-SMOW	AGI sampled
A. islandica	ACG254-1	224 m	+1.2 ‰	+0.5 ‰	11
A. islandica	ACG215-5	185.70 m	+2.9 ‰	+1.0 ‰	8
A. islandica	ACG200-13	174 m	+3.0 ‰	+0.8 ‰	13
A. islandica	ACG78-7	103.70 m	+2.5 ‰	+1.0 ‰	12
A. islandica	ACG78-1	103.70 m	+2.9 ‰	+1.0 ‰	10

B

Species	Sample number	Position	$\delta^{18}O_{sh\text{-}min}$	T_{max}	$\delta^{18}O_{sh\text{-}max}$	T_{min}	$\delta^{18}O_{sh\ max\text{-}excursion}$	$T_{max\text{-}excursion}$
G. insubrica	ACG261bis-1	235.70 m	-4.0 ‰	36.8 °C	+0.4 ‰	17.7 °C	4.4 ‰	19.1 °C
G. insubrica	ACG261-1	235.70 m	-2.7 ‰	31.1 °C	+0.3 ‰	18.1 °C	3.0 ‰	13.0 °C
G. insubrica	ACG252-1	224 m	-1.5 ‰	28.1 °C	+0.8 ‰	18.1 °C	2.3 ‰	10.0 °C

G. insubrica	ACG200-8	174 m	-0.6 ‰	25.5 °C	+1.0 ‰	18.6 °C	1.6 ‰	6.9 °C
G. inflata	ACG29bis-33	42 m	+0.5 ‰	19.4 °C	+1.6 ‰	14.7 °C	1.1 ‰	4.7 °C

Species	Sample number	Position	$\delta^{18}O_{sh\ mean\text{-}min}$	$T_{mean\text{-}max}$	$\delta^{18}O_{sh\ mean\text{-}max}$	$T_{mean\text{-}min}$	$\delta^{18}O_{sh\ mean\text{-}excursion}$	$T_{mean\text{-}excursion}$
G. insubrica	ACG261bis-1	235.70 m	-3.0 ‰	32.4 °C	-0.4 ‰	21.2 °C	2.6 ‰	11.2 °C
G. insubrica	ACG261-1	235.70 m	-2.5 ‰	30.3 °C	-0.5 ‰	21.6 °C	2.0 ‰	8.7 °C
G. insubrica	ACG252-1	224 m	-1.1 ‰	26.4 °C	+0.2 ‰	20.7 °C	1.3 ‰	5.7 °C
G. insubrica	ACG200-8	174 m	-0.6 ‰	25.5 °C	+0.6 ‰	20.3 °C	1.2 ‰	5.2 °C
G. inflata	ACG29bis-33	42 m	+0.6 ‰	19.0 °C	+1.5 ‰	15.1 °C	0.9 ‰	3.9 °C

Species	Sample number	Position	MTS	V-SMOW	AGI sampled
G. insubrica	ACG261bis-1	235.70 m	-2.3 ‰	+0.0 ‰	10
G. insubrica	ACG261-1	235.70 m	-1.8 ‰	+0.0 ‰	10
G. insubrica	ACG252-1	224 m	-0.5 ‰	+0.5 ‰	10
G. insubrica	ACG200-8	174 m	+0.2 ‰	+0.8 ‰	4
G. inflata	ACG29bis-33	42 m	+1.0 ‰	+0.5 ‰	6

Highlights

High seasonality triggered the arrival of “northern guests” in the Mediterranean Sea
Seasonality increased approaching the Middle Pleistocene Transition
Seawater temperature seasonality was the main variable of Calabrian climate change